Electron correlation effects in layered structures – a theoretical first-principles study

Inaugural-Dissertation

to obtain the academic degree
Doctor rerum naturalium (Dr. rer. nat.)

submitted to
The Department of Biology, Chemistry and Pharmacy
of Freie Universität Berlin

by
LUKAS EUGEN MARSONER STEINKASSERER
from INNSBRUCK, AUSTRIA

2017

This work was prepared under supervision of

PROF. DR. BEATE PAULUS (FREIE UNIVERSITÄT BERLIN)

from

OKTOBER 2013 UNTIL APRIL 2017

1. Reviewer:	PROF. DR. BEATE PAULUS
2. Reviewer:	PROF. DR. THOMAS RISSE
Date of the defense:	June 23th, 2017

Danksagung

Lasst mich diese Danksagung beginnen mit einer Entschuldigung, denn noch bevor ich ein Wort dieses Textes zu virtuellem Papier gebracht habe, weiß ich, dass keine meiner Worte ausreichen werden um denen die mich in den letzten vier Jahren begleitet haben gerecht zu werden.

Danke an Prof. Dr. Beate Paulus die mich stets in allen Belangen unterstützt und mir die Freiheit gegeben hat meinen eigenen Weg zu finden – ohne Sie wäre diese Arbeit nie zustande gekommen.

Danke an Prof. Dr. Thomas Risse der sich nicht nur kurzfristig bereit erklärt hat als Zweitgutachter für diese Arbeit zu fungieren, sondern durch seine Vorlesung zu den Grundlagen der Festkörperphysik auch großen Anteil daran hatte, dass ich mich diesem Thema die letzten Jahre über gewidmet habe.

Danke an Dr. Jean Christophe Tremblay dafür, dass er immer ein offenes Ohr für meine Fragen hatte.

Danke an all die Mitglieder der AG Paulus, AG Keller und AG Trembley insbesondere PD Dr. Dirk Andrae und J.Prof. Dr. Bettina Keller die mir stets mit Rat und Tat zur Seite standen sowie Julija Djordjevic für all die organisatorische Hilfe.

Danke an die Mitarbeiter der Zentraleinrichtung für Datenverarbeitung und des Hochleistungsrechenzentrums Nord, insbesondere Dr. Boris Proppe, Dr. Loris Bennett, Robert Schüttler, Dr. Holger Naundorf und Dr. Christian Tuma für all die Rechenzeit und technische Unterstützung.

Danke an die Max Planck Gesellschaft, insbesondere Bettina Menzel für all die organisatorische Hilfe und Dr. Tobias Kampfrath dafür, dass ich Teil der IMPRS sein

durfte. Auch möchte ich allen Mitgliedern der IMPRS für die gemeinsame Zeit danken – besonders der Aufenthalt in Ringberg wird mir für immer positiv in Erinnerung bleiben.
Danke an die Studienstiftung des deutschen Volkes für das fantastische Doktorandenforum in Potsdam, die Chance in der Kommission eines Auswahlverfahrens sein zu dürfen und nicht zuletzt für die finanzielle Unterstützung.
Danke an die DFG für ihre Förderung und an Dr. Elena Voloshina und die AG Fonin der Uni Konstanz, insbesondere Julia Tesch, für die angenehme Zusammenarbeit.
Danke an all jene mit denen ich zusammenarbeiten durfte, insbesondere Alessandra Zarantonello und Simon Suhr.
Thank you so much to Assoc. Prof. Nicola Gaston who was the most wonderfull host one could which for and with whom I shared many long and thought provoking talks.
Thank you also to Dani Metin, Dr. Udbhav Ojha, and James Whaanga with whom I had a wonderful time, both in Wellington and at Quaccs.

Meiner Familie, meiner Mama Astrid, meinem Vater Martin, Leopold, meinen Brüdern Mathias, Jakob und Lorenz, meinen Schwestern Sophia, Lena, Hannah und Verena, meinem Neffen Tobias, Birgit meiner Oma Cecilia und all meinen Tanten, Onkels, Cousins und Cousinen – danke dass des olm fi mi då sat. Ohne enk ware heint et were bin - des wisst går et wie viel des må bedeitit.

Carmen, die das Wunder fertig gebracht hat mich nicht nur über die letzten vier Jahre, sondern auch während meines gesamten Studiums täglich auszuhalten und in Stunden der Frustration und des Selbstzweifels eben so an meiner Seite zu sein, wie in denen der Freude – i lieb die ibo ålls.

Meinen vielen Freunden die meine Zeit hier in Berlin zu der besten meines Lebens gemacht haben (ohne irgendwelche Ordnung): Vincent, Gunter, Hotte, Marcel, Edoardo, Lisa, Jaika, Gesche, Florian, Tine, Jule, Madlen, Davood, Julia - ihr seit die besten Freunde die man sich wünschen kann!

Contents

List of Figures

Abstract

2D materials and layered structures build from them (vdWHs), are made ideal targets for computational material science by the enormous variety of structures they allow for. This great freedom is though accompanied by almost equally great challenges as the weak interactions present within vdWHs, which are the origin of many of their fascinating properties, are theoretically difficult to describe, requiring the use of sophisticated computational methods.

The starting point of my investigation were boron-nitride (BN) containing vdWHs. Using local correlation methods I studied interactions within graphane/BN vdWHs, whereby special focus was given to the effects of dispersive and mean-field (i.e. Hartree-Fock) interactions on the interlayer binding behavior. Further I investigated the effect of external electric fields on the the systems' electronic structure. Using G_0W_0 I subsequently focused on excitation energies in phosphorene/BN vdWHs. In both these cases, a delicate interplay between dispersive and mean-field interactions could be observed, resulting in interesting effects on the graphane/BN binding behavior as well as phosphorene–BN distance-dependent excitation energies. Additionally, I performed studies on the Ag(111) and Au(111) adsorption of graphene, in close collaboration with experimental partners from the university of Konstanz. These investigations were done using semi-empirical methods to account for vdW interactions. While they gave generally good agreement with the experimental findings, they at the same time demonstrated the shortcomings of the semi-empirical approach, as no method consistently outperformed all others.

Another thin film material I investigated was Gadolinium nitride (GdN), whose

large magnetic moment and properties as a semi conductor, make it an attractive material for use in spintronics. Using hybrid-DFT methods I studied the electronic structure of both bulk GdN and its (111) surface. While bulk GdN shows the aforementioned finite band gap, the formation of the (111) surface leads to the appearance of metallic surface states in the majority spin channel as well as the formation of an electron pocket in the minority spin channel which is located in center of the slab model.

Aside from the study of known structures, a second major focus of my work was the exploration of new 2D materials. Using G_0W_0 and BSE, I investigated partially brominated/chlorinated fluorographene derivatives – particularly with respect to their optical properties. Via calculation of their band structures and adsorption spectra I was able to show some of these materials to possess promising characteristics for use in photovoltaics. Cyanated graphene derivatives were also investigated and, using electron-transport calculations, I could demonstrate BN-adsorbed cyanographone to show a strong and selective detector-response to CO adsorption in the presence of N_2, CO_2 and O_2, making the material a potentially potent gas sensor.

Kurzzusammenfassung

2D Materialien sowie aus ihnen bestehende Schichtstrukturen (vdWHs) stellen durch die Vielfalt an möglichen Stoffen ein ideales Forschungsgebiet für die computergestützte Materialforschung dar. Dieser großen Freiheit stehen jedoch fast ebenso große Herausforderungen gegenüber. Da ihre Untersuchung nur mithilfe rechnerisch aufwendiger Methoden möglich ist, sind es eben jene schwachen Wechselwirkungen die vdWHs zu einem so faszinierenden Forschungsgebiet machen, welche ihre theoretische Erforschung erschweren.

Als Ausgangspunkt für meine Untersuchungen dienten Bornitrid (BN) enthaltende vdWHs. Mithilfe lokaler Korrelationsmethoden untersuchte ich Wechselwirkungen innerhalb von Graphan/BN Schichtstrukturen, wobei das Hauptaugenmerk auf den Auswirkungen dispersiver und molekularfeldtheoretischer (also auf Hartree-Fock Niveau beschriebener) Wechselwirkungen auf das Bindungsverhalten, sowie dem Einfluss externer elektrischer Felder auf die Elektronenstruktur der Systeme lag. Unter Verwendung der G_0W_0 Methode untersuchte ich in der Folge des Weiteren die Anregungsenergien in Phosphoren/BN vdWHs. In beiden Fällen konnte ein delikates Wechselspiel dispersiver sowie molekularfeldtheoretischer Wechselwirkungen beobachtet werden, welches zu interessanten Effekten im Graphan/BN Bindungsverhalten bzw., der Phosphoren–BN abstandsabhängigen Bandlücke führte. In enger Zusammenarbeit mit Experimentatoren der Universität Konstanz, führte ich außerdem eine Untersuchung zu Ag(111) sowie Au(111) Adsorption von Graphen durch. Hier kamen semi-empirischem Methoden zum Einsatz, welche auf der einen Seite sehr gute Übereinstimmung mit dem experimentellen Daten hervorbrachten,

andererseits jedoch auch die Schwächen dieses Ansatzes deutlich machten da keine der Methoden konsistent bessere Ergebnisse lieferte.

Als weiteres Dünnschichtmaterial untersuchte ich Gadolinium-nitrat (GdN), eines aufgrund seines großen magnetischen Moments, sowie seiner Eigenschaften als Halbleiter attraktiven Stoffes für die Anwendung in der Spintronik. Mithilfe von Hybrid-DFT Methoden untersuchte ich die Unterschiede in der Elektronenstruktur zwischen dem Feststoff und dessen (111) Oberfläche. Währen der GdN Feststoff eine Bandlücke aufweist, treten an der (111) Oberfläche metallische Zustände im Majoritäts-Spin, sowie eine im Zentrum des Oberflächenmodells lokalisierte Elektronen-Tasche im Minoritäts-Spin auf.

Neben der Erfoschung bekannter Strukturen, war die Erforschung neuer 2D Materialien eines der Hauptziele meiner Arbeit. Unter Zuhilfenahme von G_0W_0 sowie BSE untersuchte ich die Eigenschaften partiell bromierter/chlorierter Fluorographen-Derivate insbesondere im Bezug auf deren optischen Eigenschaften. Anhand der Berechnung ihrer Bandstrukturen und Adsorptionsspektren konnte ich zeigen, dass einige dieser Stoffe vielversprechende Merkmale für die Nutzung in Solarzellen aufweisen. Auch cyanierter Graphen-Derivate wurden untersucht. Mithilfe von Elektronentransport-Rechnungen konnten ich zeigen, dass die BN-adsorbierte Form des Cyanographon, eine starke und selektive Detektorantwort auf die Adsorption von CO in der Gegenwart von N_2, CO_2 und O_2 aufweist, welche es zu einem potentiell leistungsfähigen Sensormaterial macht.

Chapter 1

List of Publications

1.1 Main Publications

M1: Strong 1D localization and highly anisotropic electron-hole masses in heavy-halogen functionalized graphenes

L. E. Marsoner Steinkasserer, A. Zarantonello, and B. Paulus

Phys. Chem. Chem. Phys. **18**, 36, 25629-25636 (2016)

DOI: 10.1039/C6CP05188J

M2: Cyanographone and Isocyanographone – two asymmetrically functionalized graphene pseudohalides and their potential use in chemical sensing

L. E. Marsoner Steinkasserer and B. Paulus

ArXiv preprint arXiv:1703.08582 (2017)

M3: Hybrid density functional calculations of the surface electronic structure of GdN

L. E. Marsoner Steinkasserer, B. Paulus, and N. Gaston

Phys. Rev. B **91**, 23, 235148 (2015)

DOI: 10.1103/PhysRevB.91.235148

M4: Structural and electronic properties of graphene nanoflakes on Au (111) and Ag (111)

J. Tesch, P. Leicht, F. Blumenschein, L. Gragnaniello, M. Fonin, L. E. Marsoner Steinkasserer, B. Paulus, E. Voloshina, and Y. Dedkov

Sci. Rep. **6**, 23439 (2016)

DOI: 10.1038/srep23439

M5: Weak interactions in Graphane/BN systems under static electric fields - A periodic ab-initio study

L. E. Marsoner Steinkasserer, N. Gaston, and B. Paulus

J. Chem. Phys. **142**, 15, 154701 (2015)

DOI: 10.1063/1.4917170

M6: Band-gap control in phosphorene/BN structures from first-principles calculations

L. E. Marsoner Steinkasserer, S. Suhr, and B. Paulus

Phys. Rev. B **94**, 125444 (2016)

DOI: 10.1103/PhysRevB.94.125444

1.2 Other Publications

Impact of the metal substrate on the electronic structure of armchair graphene nanoribbons

L. E. Marsoner Steinkasserer, B. Paulus, and E. Voloshina

Chem. Phys. Lett. **597**, 597, 148-152 (2014)

DOI: 10.1016/j.cplett.2014.02.038

Chapter 2

Introduction

The resurgence of low dimensional materials has arguably been one of the dominating themes in material science over the last decade, impacting fields and sparking the imagination of researchers far beyond the confines of the physics community. It is generally accepted that the starting point of this revolution can be traced back to the seminal paper by Geim and Novoselov [1], who were the first to successfully demonstrate the isolation of monolayer graphite (graphene). While the properties of graphene had been studied theoretically as early as 1947 [2], its successful isolation in 2004 took the scientific community by surprise as 2D materials, such as graphene, had long been thought to be thermodynamically unstable. 70 years before Geim's and Novoselov's discovery, Landau and Peierls had both argued that strictly 2D materials simply could not exist [3, 4]. Their argument was based on the observation that, at any finite temperature, thermal fluctuations in low-dimensional crystals should lead to atomic displacements of such magnitude that they become comparable to interatomic distances, thereby leading to the disintegration of the crystal itself [5, 6]. So why did Geim and Novoselov succeed when they clearly should not have? A number of explanations have been put forward to explain the apparent discrepancy between experimental fact and theory: Some pointing to long-range *crumbling* of the 2D layer in the third dimension [7, 8] while others have argued that 2D materials are quenched in a metastable state because they are extracted from 3D

systems with their small size and strong interatomic bonds protecting them from thermal disintegration [5, 6, 9]. Be this as it may, the *rise of graphene*, as it was so aptly termed by Geim and Novoselov [6], has let to the discovery and rediscovery of a whole *zoo* of 2D materials. Some, such as hexagonal boron-nitride (BN) [10–12] or molybdenum disulfide (MoS_2) [13–15] had been well-known for decades and used as lubricants, but were *rediscovered* as 2D materials and are now heavily studied for a variety of applications which, in the case of MoS_2, range from water splitting over nanoscale transistors to solar cells [16–29]. Others were only recently isolated for the first time as e.g. phosphorene [30–37], silicene [38–45], and stanene [46–58], which are the two-dimensional forms of phosphorus, silicon, and tin, respectively. All of these materials, as well as many others, have attracted great attention from both experimental and theoretical researchers and promise to greatly impact scientific and technological developments for decades to come [59].

Aside from the introduction of novel elements into the *2D cookbook*, a very intriguing approach to modifying and custom-tailoring the properties of 2D systems to specific applications consists in the chemical i.e. covalent modification of existing structures [60–73]. While all of the above-mentioned materials have been studied in this respect, chemical modification of graphene and in particular its *halogenation* i.e. reaction with F, Cl, Br, I and H (which for simplicity we will include here under our definition of *halogens*) has probably attracted the greatest attention [64–67, 71–76]. They have the potential of not only producing new and fascinating structures, but also potentially allow to overcome some of the major problems still plaguing pristine graphene as e.g. the absence of a finite-sized band gap which has so far hindered graphene's wide-spread application in transistor technology, its otherwise superb electronic properties notwithstanding [77]. Though graphene halogenation holds great promise, it itself is obviously not free of problems. While saturation by halogens does indeed open a band gap within graphene, fully hydrogenated, fluorinated, and chlorinated graphene derivatives (graphane, fluorographene and

chlorographene) all show band gaps typical of insulators or wide band gap semiconductors, making them unattractive for electronic applications. Apart from fluorographene, direct halogenation of pristine graphene has further been proven difficult due to the inherent low reactivity of graphene [67, 78]. A possible solution to this problem consists in the use of the more reactive fluorographene as a starting material. Chemical protocols for its conversion into different graphene derivatives have recently become available [69, 78, 79] and have already been used to create fascinating materials such as room-temperature, purely organic magnets [68]. With synthetic procedures finally bridging the gap between graphene and so-called *graphene molecules* [79–81], they open up an enormous field of possible chemical graphene functionalization which promises to find applications in fields ranging from nanoelectronics to medicinal chemistry.

As thus more and more 2D materials continue being discovered and synthetic procedures are being established, making their practical use more attainable, research has started to expand, from the investigation of isolated layers, to include more complex, *stacked* structures made up of a number of different 2D materials. Layers within these structures generally only bind to one-another via weak, van der Waals (vdW) forces, making it possible to easily stack different types of materials without the need for lattice-matching. Though the interactions between the individual layers are weak, they can still have a considerable influence on a system's properties, even leading to the emergence of new properties not present in the constituting monolayers [82, 83]. While initial research into the potential of these so-called *van der Waals heterostructures* (vdWHs) is still in its infancy, researchers have already begun to exploit some of their potential e.g. in the creation of interlayer excitons [84–87] with promising applications in solar cells and light-emitting diodes.

Another possible application of vdWHs (e.g. combined graphone/BN [88] and Co/graphene/BN structures [89, 90]) consists in their use as spintronic devices offering the potential to greatly amplify modern-day computing capabilities by exploit-

ing spin information within electronic circuits. A very promising candidate for use in spintronics is GdN, who's large magnetic moment and semiconducting ground state makes it almost ideally suited for a number of important uses [91]. Though practical applications are still hindered by difficulties in its preparation, renewed interest in the material itself as well as the enormous advances made in the preparation of other 2D materials which might be used as stabilizers, make the construction real-world devices within the coming years more attainable then ever.

From a purely theoretical point of view vdWHs are both fascinating as well as challenging. While the great variability of combinations and the relatively low complexity of the individual 2D layers make them an appealing playground for theoretical chemists and physicists, the lack of enforced lattice matching leads to the emergence of large-scale Moiré patterns which are difficult to account for computationally, requiring the use of very large unit cells. Another problem lies in the description of the weak interactions themselves. Nowadays a series of methods exist to approximately account for vdW interactions within the framework of density functional theory (DFT), most famously those proposed by Stefan Grimme and coworkers [92–94], Alexandre Tkatchenko and Matthias Scheffler [95], the highly parametrized *Minnesota functionals* of Truhlar *et al.* [96–99], and the vdW-DF approach by Dion and coworkers [100–102]. Nonetheless, their accurate, non-empirical description requires high-level methods such as Møller-Plesset perturbation theory [103–107], coupled-cluster methods [108, 109] or approaches based on the adiabatic-connection fluctuation-dissipation theorem within the random-phase approximation [110–118]. These latter methods generally show poor scaling with respect to system size, though the problem can partially be overcome by local approaches such as the cluster-based method of increments [119–123] or the periodic local-MP2 method [124–126].

Computational difficulties are by no means limited to the ground state. Even more so than in 3D systems, the accurate computation of e.g. the optical properties of

2D materials requires the use of methods capable of describing electron correlation. This is due to the fact that electrons experience much lower screening in 2D as compared to 3D systems, causing a relative worsening in the quality of results obtained from mean-field approaches. Within solid state physics, the most prominent methods used to improve upon the DFT description of a systems optical properties are the *GW* and BSE methods which respectively allow to account for the effects electron–electron and electron-hole interactions on the optical spectra. Though both of these methods are noways widely used and implemented in a number of different software packages [115, 127–147] they, just as other many-body methods, generally show poor scaling with system size. Furthermore, both of them are most commonly implemented using plane-wave basis sets to represent the wave functions which causes problems for low-dimensional materials as large amounts of (computationally demanding) vacuum must be included in order to separate systems from their periodic images along non-periodic directions.

Chapter 3

Theory

> *"The underlying physical laws necessary for the mathematical theory of a large part of physics and the whole of chemistry are thus completely known, and the difficulty is only that the exact application of these laws leads to equations much too complicated to be soluble. It therefore becomes desirable that approximate practical methods of applying quantum mechanics should be developed, which can lead to an explanation of the main features of complex atomic systems without too much computation."*
>
> — P. A. M. Dirac – 1929 [148]

As so aptly expressed by Paul Dirac in his famous quote, the great number of theoretical insights, gained rapidly since the very early days of quantum mechanics, stand in stark contrast to the enormous practical difficulties that plague the subject. Indeed, even now, almost 90 years after Dirac declared the laws governing all of chemistry to be fully understood, computational chemists still need to rely on rather simplified models to simulate the complicate undertakings of their experimental colleagues. These persisting problems notwithstanding, the great potential offered by what is nowadays often called *in silico science* has spurred a number of theoretical break-troughs over the past decades, bringing the world envisioned by Paul Dirac ever closer to becoming a reality.

There is though, as of now, no one-size-fits-all solution to the problems faced by

theoretical chemists and material scientists, making it necessary to carefully weight needed accuracy versus available resources when choosing the appropriate method to be applied to a particular problem.

In the following, I will lay out the principles behind the techniques used in this thesis while referring the reader to the literature should he or she require more detailed information. In order to simplify the notation, I will only discuss the closed-shell, i.e., spin-paired formulations of the methods. The extension to expressions including spin is in most cases straightforward and further amply laid out in the cited literature. Also, for the sake of clarity, the following derivations will exclusively use atomic units[1].

3.1 Mean field methods

As alluded to previously, excluding relativistic effects, most questions encountered within the realm of chemistry and/or material science can in principle be answered by solving a system's (time-dependent) Schrödinger equation [149]

$$i\frac{\partial \Psi}{\partial t} = \mathcal{H}\Psi \tag{3.1}$$

where $\mathcal{H}$ is the systems Hamiltonian and Ψ its many-body wave function. In practice, the solution to this equation is though in most cases far too complicated to be attempted directly, and so methods have to be construed to make the problem more palpable. Two basic simplifications that are both applicable to a large number of systems and highly useful in lowering the complexity of eq. (3.1) are:

1. Assuming the Hamiltonian to contain no explicitly time-dependent terms.

2. Separating the total Hamiltonian into a nuclear and an electronic contribution

[1] The following physical constants are all unity by definition: $\hbar$, m_e, e, $1/4\pi\varepsilon_0$. $\hbar$ here is the reduced Plank constant ($h/2\pi$), m_e the electron rest mass, e the elementary charge and ε_0 the vacuum permittivity.

and neglecting non-adiabatic coupling terms between the two.

While the applicability of the first approximation depends on the type of system and properties being studied, the second, known as the Born-Oppenheimer approximation [150], derives its justification from the high mass ratio between nuclei and electrons which results in an equally large difference in average velocities. This leads to the electrons reacting almost instantaneously to any movement by the nuclei. Both these considerations let us reformulate the problem in terms of what is called the time-independent electronic Schrödinger equation

$$H\Psi = E\Psi \tag{3.2}$$

where we have omitted the superscripts *el* for brevity. Even this equation is though generally much too complicated to solve, and further approximations must be made, if one wishes to proceed. A very attractive approximation both due to its mathematical simplicity as well as physical insight is the assumption that, while eq. (3.2) describes a system of mutually interacting particles, their behavior can to a large degree be captured by assuming them to be independent from one-another, only experiencing the presence of all other particles in the system via a so-called *effective potential* (v_{eff}).

Mathematically this corresponds to the introduction of one-particle operators (h_i) with the total Hamiltonian (H) being given by the sum over all h_i and a constant internuclear potential V_{NN} as

$$H = \sum_i h_i + V_{\text{NN}} \tag{3.3}$$

The one-particle wave functions ψ_i, associated with h_i satisfy

$$h_i\psi_i = \left[T_i + v_{\text{eff}}\right]\psi_i = \epsilon_i\psi_i \tag{3.4}$$

where T_i is the kinetic energy operator for electron i i.e. $T_i = -\frac{1}{2}\nabla_i^2$ and ϵ_i is the eigenvalue of h_i corresponding to the eigenfunction ψ_i. In the context of electronic structure theory, the one-electron wave functions ψ_i are generally referred to as *electronic orbitals* (or simply *orbitals* for short). The total electronic wave function Ψ is then given by the antisymmetrized product

$$\Psi = A\prod_{i}^{N}\psi_i \tag{3.5}$$

where A is the antisymmetrization operator defined as

$$A = \frac{1}{N!}\sum_{\Pi}(-1)^{n_p}\Pi \tag{3.6}$$

with the sum running over all permutations of the electrons (Π) and n_p the number of elementary (two-particle) permutations in Π.

The need to employ the antisymmetrization operator [2] arises from the fermionic nature of electrons [151] which leads to the requirement that the electronic wave function change its sign if two electrons are interchanged. An analogous theory can readily be formulated for the case of bosons by simply interchanging the antisymmetrization with a symmetrization operator in eq. (3.5). In the literature the antisymmetrized wave function is often referred to as a *Slater determinant* after John C. Slater [151] since it can be conveniently written in the form of a determinant containing the electronic orbitals.

Having reduced the complexity of eq. (3.2) from the solution of an N-particle problem down to that of solving N one-particle problems, one can now attempt to solve eq. (3.4), thereby obtaining an approximate solution to the complex many-body problem (3.2).

Several forms exist for the eq. (3.4) reflecting different physical and mathematical

[2] A simple product of ψ_i's would in principle also fulfill the requirement of being an eigenfunction to eq. (3.3).

approaches. We will here briefly focus on the two major methods employed in theoretical chemistry and material science, i.e., the Hartree-Fock method (HF) [152] as well as Kohn-Sham density functional theory [153, 154] (KS-DFT). Though the latter is nowadays the more popular approach in practice, we will begin our discussion with the former due to its immediate physical appeal as well as formal closeness to the original problem.

3.2 Hartree-Fock

The HF method can be derived directly from the N-particle Schrödinger eq. (3.2) by inserting the antisymmetrized product ansatz (3.5). Within HF theory, the effective potential in eq. (3.4) is then given by

$$v_{\text{eff}}^{\text{HF}}(\mathbf{r}_1) = F(\mathbf{r}_1) - T_1(\mathbf{r}_1) = -\sum_{\alpha} \frac{Z_\alpha}{r_{1\alpha}} + \sum_{j=1}^{N/2} \left(2J_j(\mathbf{r}_1) - K_j(\mathbf{r}_1)\right) \tag{3.7}$$

where $\mathbf{r}$ is used as a place holder for all three spacial coordinates of the particle, the sum over α runs over all atomic nuclei and $r_{1\alpha} = |\mathbf{r}_1 - \mathbf{R}_\alpha|$. $F(\mathbf{r}_1)$ is usually referred to as the *Fock operator*. The two-electron contributions to F, i.e., J and K are the Coulomb and exchange operator respectively and are given by

$$J_j(\mathbf{r}_1)\psi_i(\mathbf{r}_1) = \int d\mathbf{r}_2 \psi_j^*(\mathbf{r}_2) \frac{1}{r_{12}} \psi_j(\mathbf{r}_2)\psi_i(\mathbf{r}_1) \tag{3.8}$$

$$K_j(\mathbf{r}_1)\psi_i(\mathbf{r}_1) = \int d\mathbf{r}_2 \psi_j^*(\mathbf{r}_2) \frac{1}{r_{12}} \psi_i(\mathbf{r}_2)\psi_j(\mathbf{r}_1) \tag{3.9}$$

Given that these operators depend on the electronic orbitals themselves, directly finding the eigenfunctions and eigenvalues to the HF Hamiltonian is in general not possible. One can however circumvent this problem by applying the variational principle which states that the systems' true ground state energy constitutes a lower

bound to the expectation value

$$E \leq \frac{\langle \tilde{\Psi} | H | \tilde{\Psi} \rangle}{\langle \tilde{\Psi} | \tilde{\Psi} \rangle} \tag{3.10}$$

where $\tilde{\Psi}$ is a so-called *trial* function and E is the true ground state energy of the system. One can therefore obtain a best-fit solution to the eigenvalue problem by variationally changing the trial functions $\tilde{\Psi}$ (via changes in the orbitals ψ_i) until the energy does not vary to within a predetermined threshold. The orbitals constituting the *trial* function are generally themselves expressed as a linear combination of additional auxiliary functions called *basis functions* and the problem is recast as finding the matrix of coefficients that yields the lowest-energy linear combination of the basis functions [155, 156]. Basis functions and their properties will be discussed in more detail later (see subsection 3.8.1 Basis sets).

While the HF method generally performs rather poorly in predicting the properties of real world systems [152], it is made attractive by the fact that it can be derived directly from first principles without the need for parametrization. It is self-interaction free and contains an exact description of the exchange-interaction between electrons which is a direct result of the wave function antisymmetry. It can further be extended upon in a number of ways to include effects not captured within the single determinant approximation, such as, explicit electron–electron interaction beyond exchange, also known as *electron correlation*. We will discuss two of these extensions which improve upon HF via the use of Rayleigh-Schrödinger perturbation theory as well as partial summation techniques at a later point (see subsection 3.5.1 MP2 and section 3.6 *GW*). More details on the HF method itself as well as its implementation in the electronic structure code CRYSTAL14 [157, 158] can be found in ref. [152, 159, 160]. Finally, let us note an important result retaining to the physical meaning of the eigenvalues to the Fock operator. As has been shown by Tjalling C. Koopmans [161], the eigenvalues belonging to *occupied* HF orbitals approximate the

negative ionization potentials of the system. The result was later extended to virtual orbitals which approximate electron affinities [162, 163]. This has some important consequences which will be discussed later (see subsection 3.5.1 MP2 and section 3.6 *GW*).

3.3 Density functional theory

Let us now turn our attention to the second method alluded to earlier, namely Kohn-Sham density functional theory (KS-DFT) [153, 154]. While the HF method is obtained directly from the electronic Schrödinger equation, the derivation of KS-DFT is somewhat more involved. Its basis is formed by two seminal theorems proven by Pierre Hohenberg and Walter Kohn in 1964 [154]. Together they demonstrate both the existence of a functional, uniquely connecting the ground state electron density

$$\rho(\mathbf{r}) = N \int d\mathbf{r}_2 \cdots \int d\mathbf{r}_N \Psi^*(\mathbf{r}_1, \mathbf{r}_2, \cdots, \mathbf{r}_N)\Psi(\mathbf{r}_1, \mathbf{r}_2, \cdots, \mathbf{r}_N) \tag{3.11}$$

to the ground state energy of a system, and the existence of a variational principle for the electron density, that is, the fact that the ground state electron density minimizes the systems' energy. While the original formulation by Hohenberg and Kohn only holds for non-degenerate ground states, it was later generalized by Mel Levy [164, 165].

While the Hohenberg-Kohn theorems establish the theoretical basis for the use of the electron density (3.11) in place of the N-electron wave function, proving the *existence* of a unique functional connecting the two, they do not provide us its exact mathematical form. Progress in this direction was made shortly afterwards, when Walter Kohn and Lu Jeu Sham proposed a mapping of the true interacting N-electron system to a fictitious *non-interacting* system. Within Kohn-Sham DFT, the systems'

energy as a functional of the density ($E[\rho]$) can then be written as

$$E[\rho] = \int \mathrm{d}\mathbf{r}\rho(\mathbf{r})v_{ext}(\mathbf{r}) + T_\mathrm{s}[\rho] + E_\mathrm{H}[\rho] + E_\mathrm{xc}[\rho] \tag{3.12}$$

Here, v_{ext} is the external potential of the interacting system, i.e., the electron-nuclear interaction, possible external electric fields etc., $T_\mathrm{s}[\rho]$ is the Kohn-Sham kinetic energy operator

$$T_\mathrm{s}[\rho] = -\frac{1}{2}\sum_i^N \int \mathrm{d}\mathbf{r}\phi_i^*(\mathbf{r})\nabla^2\phi_i(\mathbf{r}) \tag{3.13}$$

E_H is the Hartree energy which is given as a functional of the density by

$$E_\mathrm{H}[\rho] = \frac{1}{2}\int \mathrm{d}\mathbf{r}_1 d\mathbf{r}_2 \frac{\rho(\mathbf{r}_1)\rho(\mathbf{r}_2)}{r_{12}} \tag{3.14}$$

and $E_\mathrm{xc}[\rho]$ is the exchange-correlation functional which is the only unknown quantity within Kohn-Sham DFT. The Kohn-Sham effective potential can now be obtained as

$$v_\mathrm{eff}(\mathbf{r};N) = v_{ext}(\mathbf{r};N) + \left.\frac{\delta E_\mathrm{H}[\rho]}{\delta\rho(\mathbf{r})}\right|_N + \left.\frac{\delta E_\mathrm{xc}[\rho]}{\delta\rho(\mathbf{r})}\right|_N \tag{3.15}$$

The last term in this equation, i.e.,

$$v_\mathrm{xc}(\mathbf{r};N) = \left.\frac{\delta E_\mathrm{xc}[\rho]}{\delta\rho(\mathbf{r})}\right|_N \tag{3.16}$$

is the so-called exchange-correlation potential for the N-electron system. An important property of the KS-DFT exchange-correlation potential is its continuity with respect to the fractional number of electrons in the system while at integer occupations a discontinuity may emerge as

$$\Delta_\mathrm{xc} = v_\mathrm{xc}(\mathbf{r};N+\delta) - v_\mathrm{xc}(\mathbf{r};N-\delta) \tag{3.17}$$

where the limits $\delta \to 0$ are implied [166, 167]. For clarity the formal $\mathbf{r}$-dependence of Δ_{xc} was dropped as it can be shown to be a constant function of $\mathbf{r}$ [167]. The existence of this so-called *derivative discontinuity* within KS-DFT has important consequences when considering a systems' quasiparticle gap as we will see later.

The Kohn-Sham transformation finally yields a set of equations of the same form as eq. (3.4), and the N-electron problem has again been reduced to a set of N one-electron problems. Despite the striking similarities between the mathematical formalisms resulting from the two methods (HF versus KS-DFT), it is important to also stress the differences between the two approaches. The HF equations result from a rather straightforward approximation to the electronic Schrödinger equation, i.e., the ansatz of a single Slater determinant which results in neglecting all explicit electron–electron interaction except for electron-exchange. In contrast, the KS-DFT equations do not in and of themselves represent an approximation but in principle allow to *exactly* recast the N-electron problem in terms of one-particle equations as long as the *exact* form of the exchange-correlation functional $E_{xc}[\rho]$ is known. As this is in general not the case, we must find approximate forms for $E_{xc}[\rho]$. Approximations to $E_{xc}[\rho]$ are often ranked on what is called *Jacob's ladder* [168] which organizes them according to their (general) level of accuracy.

Let us now ourselves ascend *Jacob's ladder* and briefly lay out the major DFT methods used in this thesis.

On the first rung of the ladder, we find the so-called *local density approximation* (LDA) [169–171]. It assumes that the *true* exchange-correlation functional can be approximated by its homogeneous electron gas expression

$$E_{xc}^{LDA} = \int d\mathbf{r}\rho(\mathbf{r})\epsilon_{xc}^{LDA}[\rho] \tag{3.18}$$

This expression can then be divided into both an exchange and a correlation part. While the first of these had already been derived analytically by Paul Dirac in 1930

[170], the correlation part is only known in the high- and low-density limit [172] and intermediate values have to be obtained from interpolation of accurate quantum Monte Carlo results [171, 173, 174].

As LDA struggles to capture situations in which the electron density is far from homogeneous (e.g. molecules or surfaces) further flexibility needs to be incorporated into the exchange-correlation functional. The most obvious way to do so is to construct a functional which depends not only on the value of the electron density at a given point in space but also on its derivative. Given that the derivative incorporates information on the behavior of a function in the vicinity of a given point, such functionals are sometimes termed *semi-local*. As this might induce one to confuse them with true *non-local* functionals we will though refrain from using this terminology.

The inclusion of gradient-dependence into the exchange-correlation functional leads us to the GGA or *generalized gradient approximation* to DFT and with it the second rung on *Jacob's ladder*. Within GGA, the exchange-correlation functional takes the form

$$E_{\mathrm{xc}}^{\mathrm{GGA}} = \int \mathrm{d}\mathbf{r}\rho(\mathbf{r})\epsilon_{xc}^{\mathrm{GGA}}[\rho, \nabla\rho] \tag{3.19}$$

There is no unique GGA functional, and a number of different formulations have been proposed with the most famous examples being the PW91 [175] functional as well as PBE [176] and its revisions: revPBE [177], RPBE [178] and PBEsol [179].

While GGA functionals generally perform very well for metallic and covalently bound systems, they are unable to incorporate more long-range interactions such as van-der-Waals (vdW) forces and struggle to describe systems with highly-localized electron densities as occur for example in transition metal $d-$ and $f-$shells.

The problem of missing weak interactions is very difficult to solve satisfactorily with many approaches having been suggested in the literature involving varying degrees of empiricism. Examples of such methods include those proposed by Stefan Grimme and coworkers [92–94], Alexandre Tkatchenko and Matthias Scheffler [95],

and the highly parametrized *Minnesota functionals* of Truhlar *et al.* [96–99]. While the reader is referred to the literature for a detailed discussion of these methods, we will here focus on a different approach, namely vdW-DF by Dion and coworkers which we will briefly lay out later in this text. A solution to the second of the aforementioned problems, i.e., the description of highly localized systems of electrons, comes in the form of including a fraction of exact-exchange (E_{XX}), i.e., exchange calculated at the HF-level, into the definition of the exchange-correlation functional. Such functionals are called *hybrid functionals* [180] and take the general form

$$E_{xc}^{\text{hybrid}} = \int \mathrm{d}\mathbf{r}\rho(\mathbf{r})\epsilon_{xc}^{\text{GGA/LDA}}[\rho, \nabla\rho] + \zeta E_{XX} \tag{3.20}$$

Important examples of functionals using this approximation include PBE0 [181] and B3LYP [171, 182–185]. While these functionals clearly improve upon the accuracy of GGA type functionals, their high computational cost - particularly when using plane-wave basis sets - has stimulated attempts to use truncated versions of E_{XX} in the definition of the hybrid functional. The most famous of these attempts resulted in the HSE03 and HSE06 functionals by Heyd, Scuseria and Ernzerhof [186, 187] which employ an error function in r_{12}^{-1} space to restrict the exchange interaction to electrons spatially close to one another. They generally result in significant improvements over GGA's, particularly in the description of electronic band gaps. A result that has been explained by their similarity to an electron quasiparticle theory [188].

Before concluding this section, we will now briefly discuss two important examples of DFT functionals which do not strictly fall into the *Jacob's ladder* scheme but attempt to address some of the main problems present in LDA and GGA density functionals, i.e., the so-called *band gap problem*, that is their general underestimation of electronic band gaps, as well as their inability to describe *nonlocal*, long-range interactions such as van der Waals (vdW) forces.

We begin our discussion with the latter problem, i.e., the appropriate description of vdW forces. In 2004, Dion and coworkers [100] proposed a way to express non-local correlation within the DFT framework in terms of a density-density interaction formula derived using a "plasmon" pole approximation for the inverse dielectric function [101]. The resulting functional termed vdW-DF, was later refined leading, among others, to the development of the vdW-DF2 functional [101]. Both methods separate the exchange-correlation functional into an *outer* and an *inner* functional, where the *outer* functional uses GGA to account for the local exchange-correlation energy, while the *inner* functional is used to parametrize the plasmons [102]. This introduces some ambiguities into the functional [189], rendering some e.g. more applicable to molecules while others better describe condensed matter. It is therefore desirable to formulate a functional, fully based on the plasmon pole description used in the *inner* functional. This was recently achieved by Kristian Berland and Per Hyldgaard [189] and the resulting functional (called vdW-DF-CX for "consistent exchange") has been shown to yield binding energies and structural properties in excellent agreement with experimental results for a wide variety of systems.

Let us now turn to the second of the two issues mentioned above, i.e., the improper description of band gaps within LDA and GGA functionals. As a solution to this problem, we will briefly discuss the case of so-called *model potentials* specifically the case of the GLLB-SC potential [166, 190] named after O. Gritsenko, R. van Leeuwen, E. van Lenthe, and E. J. Baerend which was extensively used in this work. Note that, while we will for simplicity at some points refer to the GLLB-SC *functional*, this should always be understood to mean the GLLB-SC *potential* as there is no known functional which has the GLLB-SC *potential* is its functional derivative according to eq. (3.16). The GLLB-SC potential tries to model the exact KS potential given by the optimized effective potential (OEP) method [191, 192]. More specifically it approximates the exact-exchange optimized effective potential (EXX-OEP) which does not include correlation contributions [193]. As the name suggests, the GLLB-SC

potential is based on the simplification of the EXX-OEP proposed by Gritsenko *et al.* (GLLB) [190] which is itself an approximation to the KLI (Krieger, Li, Iafrate) potential [194]. For the correlation part, Kuisma and colleagues use PBEsol [179] to make it more suitable for use in solid state systems calling the resulting potential GLLB-SC [166]. On top of providing a better description of localized electrons, GLLB-SC allows one to directly calculate the quasiparticle gap (E_g^{QP}) of a system i.e. the difference between its ionization potential (IP) and its electron affinity (EA), given by the sum of the KS gap (E_g^{KS}) [166] and the derivative discontinuity (Δ_{xc}) defined in eq. (3.17) as

$$E_g^{\mathrm{QP}} = IP - EA = E[\rho_{N-1}] - 2E[\rho_N] + E[\rho_{N+1}] = E_g^{KS} + \Delta_{\mathrm{xc}} \tag{3.21}$$

This approach has shown [195] to yield results in excellent agreement with experimental data while keeping the computational cost to that of a "normal" GGA calculation, representing a significant increase in speed over alternatives such as the use of hybrid functionals or the *GW* method (see section 3.6 *GW*).

As a concluding remark, we note that the presence of the derivative discontinuity is an artifact of the multiplicative KS potential and explicitly orbital dependent functionals such as hybrid functionals within the generalized KS scheme, already incorporate some or all of the derivative discontinuity [196, 197]. This results in E_g^{KS} being close to E_g^{QP} in those cases, partially explaining the good agreement between experimentally observed band gaps and those obtained from hybrid functional calculations [196]. Lastly, methods formulated within a proper quasiparticle picture such as HF or *GW* do not show a derivative discontinuity and directly yield the quasiparticle gap as the difference between the highest occupied and lowest unoccupied energy levels [166].

3.4 Beyond the mean field approximation

In the previous section, we have discussed two very different methods (HF and DFT) which allow us to reformulate the N-particle problem posed by the electronic Schrödinger equation of a system with more than one electron, as a set of N one-particle problems, whose solution is computationally significantly easier. These methods have enjoyed stunning success, and several solutions have been presented over the years in order to overcome their most severe shortcomings such as the systematic underestimation of electronic band gaps as well as their inability to describe nonlocal vdW interactions. Nonetheless, all these methods still contain some level of ambiguity making it impossible to improve upon them in a systematic way, though the vdW-DFT functionals described at the end of the previous section might to a certain extend be considered an exception to this rule.

To overcome these issues and still exploit the good description provided by both, HF and DFT, a number of methods have been proposed over the years, improving upon them in different ways. Some of these were rather extensively used in this work and will therefore be (briefly) discussed here. For a more exhaustive introduction as well as other possible choices of methods see ref. [115, 152, 198–200]. We will also refrain from discussing more basic concepts such as that of Green's functions and their properties. For an introductory discussion, see the excellent book by Richard D. Mattuck [201].

3.5 MP2 and RPA

3.5.1 MP2

We will begin our discussion by the conceptually simplest of the aforementioned methods which essentially consists in applying Rayleigh-Schrödinger perturbation theory to the problem of accounting for electron–electron interactions not described

within HF. This method is known as Møller-Plesset perturbation theory [202] or MPX, where X indicates the order of expansion of the perturbation series. The most popular form of Møller-Plesset perturbation is MP2 as it combines good accuracy with relatively modest computational cost. Expansions larger than $X = 3$ on the other hand are seldom used. High-order expansions where indeed shown to be divergent in some cases [203]. In short, the method considers an unperturbed Hamiltonian H_0 which is chosen to be the *shifted* Fock operator (see eq. (3.7))

$$H_0 = F + \langle \psi_0 | H - F | \psi_0 \rangle \tag{3.22}$$

with ψ_0 an eigenfunction to the Fock operator. The perturbation is defined as the difference between the exact Hamiltonian of the system and the *shifted* Fock operator ($V = H - H_0$). One can then calculate a first correction to the mean-field energy of the system from the second order contributions as

$$E^{\mathrm{MP2}} = \sum_{i,j}^{\mathrm{occ}} \sum_{a,b}^{\mathrm{virt}} \frac{2V_{ij}^{ab} V_{ij}^{ab*}}{\epsilon_i + \epsilon_j - \epsilon_a - \epsilon_b} - \frac{V_{ij}^{ab} V_{ij}^{ba*}}{\epsilon_i + \epsilon_j - \epsilon_a - \epsilon_b} \tag{3.23}$$

with sums $\sum_{i,j}^{\mathrm{occ}}$, $\sum_{a,b}^{\mathrm{virt}}$ running over all occupied/unoccupied orbitals. The asterisk denotes the complex-conjugate and

$$V_{ij}^{ab} = \left\langle \psi_i(\mathbf{r}_1)\psi_j(\mathbf{r}_2) \left| \frac{1}{r_{12}} \right| \psi_a(\mathbf{r}_1)\psi_b(\mathbf{r}_2) \right\rangle \tag{3.24}$$

where ψ_i is the HF orbital with eigenvalue ϵ_i. For future reference we note that the first term in eq (3.23) is generally called the *direct* contribution to the MP2 energy (E^{dMP2}) while second term is referred to as *second-order exchange* (E^{SOX}) [106].

One of the major weaknesses of the MP2 method is its inapplicability to metallic systems. Indeed, its error relative to the exact solution generally grows with the polarizability of the medium [105]. The reason for this behavior can be quite readily seen from eq. (3.23). If the band gap decreases, the weight of the corresponding

terms in eq. (3.23) increases as the denominator decreases. Since the polarizability of a system is approximately inversely proportional to its band gap [132], we immediately see how for highly polarizable systems, the basic assumption that (3.23) be small as compared to the total energy breaks down. Before discussing a solution to this problem, let us make one final observation regarding the MP2 energy expression [204]. We had already discussed Koopmans' theorem in the context of the HF method (see section 3.2 Hartree-Fock) and noted that the orbital energies of occupied/virtual orbitals within HF approximate the systems IP/EA. Consequently, we can reinterpret the denominator of eq. (3.23) as approximating the energy of the double-excitation[3] $|ij\rangle \rightarrow |ab\rangle$ given by the sum of the IPs for electrons in molecular orbitals i and j minus the EAs for molecular orbitals a and b.

By doing so, we neglect three important types of interactions:

1. Attraction between electrons in orbitals a, b and holes in orbitals i, j.
2. Repulsion between electrons in orbitals a, b.
3. Repulsion between holes in orbitals i, j.

Though these interactions are less important at medium to high polarizabilities, they become crucial at low polarizabilities [205] meaning that MP2 is a good approximation only in the range of intermediate polarizabilities.

3.5.2 RPA

While the low-polarizability problem can only be overcome by more sophisticated techniques such as coupled cluster (CC) methods, the high polarizability limit can be efficiently addressed by what is known as the *random phase approximation* (RPA)[4]. The method which was originally introduced by Bohm and Pines [206–208] can be

[3] We have suppressed all non-active orbitals in the ground and excited state Slater determinant for clarity.

[4] Herein, we will always use the term RPA to refer to what in the literature is sometimes referred to as *direct* RPA, i.e., neglecting ladder diagrams (see ref. [115] for details).

introduced in a number of ways, such as a ring-approximation to the coupled cluster single-double (CCSD) equations [209, 210] and the reader is referred to ref. [115] for a detailed discussion. The connection to MP2 is made clearest by drawing the Goldstone diagrams for the correlation energy expression of both methods and comparing them to one-another[5]. The diagrams for both methods are shown in fig. 3.1, with the MP2 energy divided into its *direct* and *exchange* contribution (see (3.23)) [105–107]. We now see the reason for introducing this separation, as we compare the diagrams for the RPA energy (E^{RPA}) to the expression for the *direct* MP2 energy (E^{dMP2}). The direct contribution to the MP2 energy is nothing but the first term in the (infinite) expansion of the PRA correlation energy. The total RPA correlation energy is then obtained from a summation over *all* bubble diagrams to infinite order. These diagrams physically represent dynamic screening of the electron–electron interaction and, while the finite order expansion used in MP2 breaks down for small band gap systems, the summation to infinite order used within RPA remains applicable even to metals.

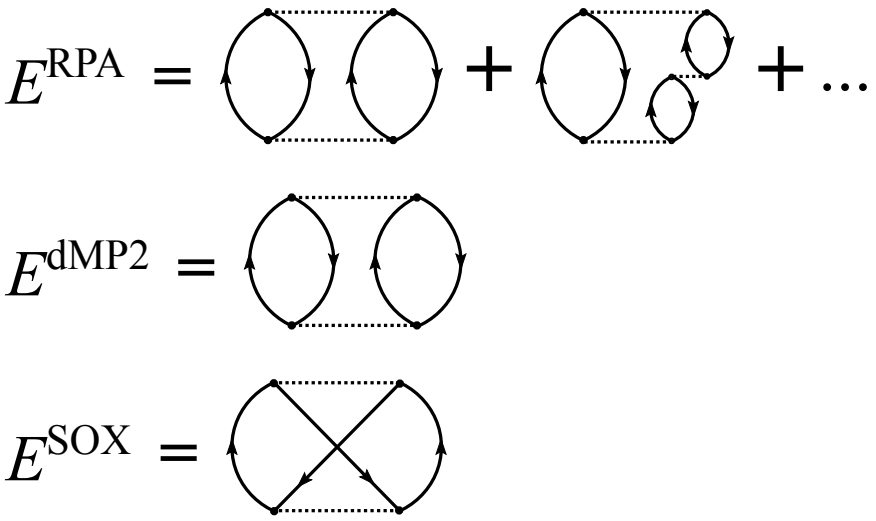

Figure 3.1: Goldstone diagrams for the *direct* (E^{dMP2}) and *second-order exchange* (E^{SOX}) contributions to the MP2 as well as the RPA correlation energy (E^{RPA}). Dotted lines correspond to the bare Coulomb interaction while full lines indicate particles/holes (see ref. [152] for details).

[5]For rules on how to evaluate Goldstone diagrams, see the book by Szabo and Ostlund [152].

Another important difference between the two methods is that the diagrams corresponding to the second-order exchange (SOX), are present in MP2 but are neglected within RPA. While for highly polarizable systems, neglecting this term has little effect, and bubble diagrams provide the dominating contribution to the correlation energy, the exchange term becomes more and more important at intermediate to low polarizabilities meaning that one should expect RPA to perform more poorly in those cases.

Finally, we note that the second order exchange term is also the reason why, contrary to RPA, MP2 is self-correlation free and exact for one-electron systems [105–107, 210–212].

3.5.3 Local MP2

We had already noted that MP2 provides relatively high accuracy combined with moderate computational costs. This together with the fact that it does not rely on any type of empirical parameters, makes it a very attractive and widely used method within molecular computational chemistry. While its computational cost is modest compared to other wave function based methods, MP2 still suffers from a formal M^5 scaling with M the number of basis functions in the basis set [213]. The method thus quickly becomes very expensive for larger systems. The problem is compounded in the periodic case by the fact that one has to consider excitations between different points in $\mathbf{k}$-space. This high computational cost of the method stands in stark contrast to the physically intuitive conclusion that, at least in non-metallic systems, electrons should be relatively localized either between pairs of atoms in the form of chemical bonds or close to individual atoms. Interaction between such localized electrons should then be rather short-ranged in nature quickly becoming insignificant as the physical distance between, e.g., two ions in a crystal increases. The reason for the bad scaling of the MP2 method thus lies primarily within the delocalized nature of the HF canonical orbitals and not necessarily the method itself.

A way to overcome this problem was suggested Pulay and Saebø in the 1980's [214–216] in the form of the so-called local MP2 (LMP2) method which exploits the locality of electron correlation by first applying a unitary transformation to the HF canonical orbitals into a localized set of orbitals, which ate then used to evaluate the MP2 energy. This is achieved using special localization methods such as those developed by Foster and Boys [217, 218] or Pipek and Mezey [219]. While Pulay and Saebø focused on molecules, their method has later been extended to periodic systems by Pisani, Schütz, Maschio, Usvyat, and others and implemented in the CRYSCOR code [124–126].

Within LMP2, the occupied space is spanned by the aforementioned localized (Wannier) functions while the unoccupied space is generally made up of so-called projected atomic orbitals (PAOs) which are constructed by applying the projection operator

$$P_{\mathrm{PAO}} = 1 - \sum_{n}^{\mathrm{occ}} |n\rangle \langle n| \tag{3.25}$$

with $|n\rangle$ the HF orbitals though other method such as e.g. orbital specific virtuals [220–224] have recently become available. The advantage of this procedure is that the total MP2 energy of a system can then be expressed as a sum over pair energies as

$$E^{\mathrm{LMP2}} = \sum_{i} \sum_{j \text{ near } i} E_{i,j}^{\mathrm{LMP2}} \tag{3.26}$$

where i runs over all Wannier functions in the unit cell and j in principle runs over all (infinitely many) Wannier functions in the infinite crystal. The accuracy and computational cost of the calculation now depends on the truncation criterion used to determine which j's are considered in the second summation.

3.6 *GW*

Though MP2 can be used to obtain single-particle excitation energies and gives good results for systems of intermediate polarizability [105–107], it is not commonly used for that purpose. The most popular way for overcoming the DFT band gap problem based on *ab-initio* methods Instead consists in the use of the so-called *GW* method. It was originally proposed by Hedin [225] and first applied to real materials by Godby, Schlüter, and Sham [226], as well as Hybertsen and Louie [227]. The approximation can be derived directly from what are known as Hedin's equations [225, 228, 229] which in principle represent an *exact* one-particle reformulation of the many-electron problem [152]. The equations are

$$\text{self-energy:} \quad \Sigma(1,2) = i \int \mathrm{d}(3,4) G(1,4) W(1^+,3) \Gamma(4,2;3) \tag{3.27}$$

$$\text{screened potential:} \quad W(1,2) = V(1,2) + \int \mathrm{d}(3,4) V(1,3) P(3,4) V(4,2) \tag{3.28}$$

$$\text{polarization:} \quad P(1,2) = -i \int \mathrm{d}(3,4) G(2,3) \Gamma(3,4;1) G(4,2) \tag{3.29}$$

$$\text{vertex function:} \quad \Gamma(1,2;3) = \delta(1,2)\delta(1,3) + \int \mathrm{d}(4,5,6,7) \frac{\delta \Sigma(1,2)}{\delta G(4,5)} G(4,6) G(7,5) \Gamma(6,7;3) \tag{3.30}$$

where we have used (i) as shorthand for $(\mathbf{r}_i, t_i)$, $V(1,2) = V(\mathbf{r}_1, \mathbf{r}_2)\delta(t_1 - t_2)$ is the Coulomb potential, Σ is the self-energy and the superscript $^+$ indicates the time index is shifted forward by an infinitesimal amount. Note that the polarization (P) is directly connected to the dielectric function (ε) as $\varepsilon = 1 - VP$. Hedin's equations can in principle be solved self-consistently, along with the Dyson-Schwinger equation

$$G(1,2) = G_0(1,2) + \int \mathrm{d}(3,4) G_0(1,3) \Sigma(3,4) G(4,2) \tag{3.31}$$

by starting from G_0, and iterating until the self-energy converges. Due to their complicated nature, this is though almost always impossible to do in practice. We note for completeness that, while in the above equation, G_0 corresponds to $\Sigma = 0$, in practice G_0 is usually taken from $H_0 = H^{\text{Hartree}} + V^{\text{xc}}$ where V^{xc}, is some local and energy-independent exchange-correlation potential [200]. This is done by simply substituting Σ in eq. (3.31) by $\Delta\Sigma = \Sigma - V^{\text{xc}}$.

A simple, yet physically sensible, and extremely useful approximation can be made to Hedin's equations by setting $\Gamma = \delta(1,2)\delta(1,3)$, i.e., ignoring the second term in the vertex function in eq. (3.30). This leads to the polarization being given by $P = -\text{i}GG$ and a self-energy equal to $\Sigma = iGW$. This approximation is generally called the GW-approximation. While ignoring the vertex in eq. (3.30) might seem arbitrary at first, the physical significance of this step becomes clearer if we compare the resulting expression for the self-energy to that of the HF-method. The HF self-energy (Σ^{HF}) is given by $\Sigma^{\text{HF}} = iGV$ as compared to the GW self-energy $\left(\Sigma^{GW} = iGW\right)$ in which the bare Coulomb potential V is substituted by the screened interaction W. Hence, while within the HF-method, electrons only interact through Hartree- and exchange-interaction (terms J and K in eq. (3.7)), electron correlation is explicitly taken into account within the GW approximation through the inclusion of screening of the electron–electron interaction by the surrounding medium via the dielectric function (ε).

As it turns out, electron correlation can to a large extent be captured by screening (in particular for weakly correlated systems) rendering the replacement of V by W an excellent approximation to the true self-energy. For clarity, the Feynman diagrams for the Dyson-Schwinger equation as well as the self-energy expressions within the HF and GW approximations are shown in fig. 3.2. The figure also shows the expression for the RPA screened interaction (W_0 in fig. 3.2) which is used for all calculations performed in this work.

Before moving on to discussing some further approximations which make the

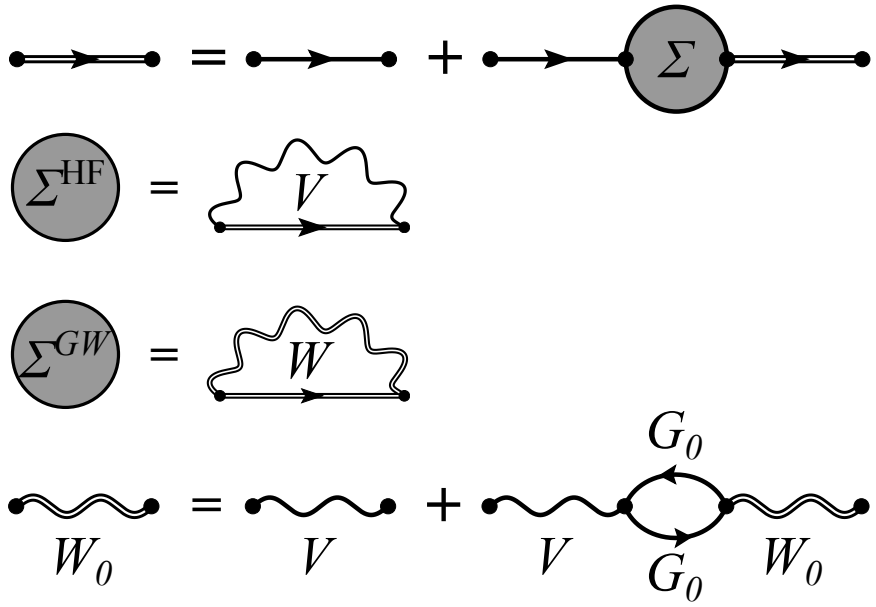

Figure 3.2: Feynman diagrams for the Dyson-Schwinger equation as well as the self-energy expressions within the HF (see section 3.2 Hartree-Fock) and *GW* (see section 3.6 *GW*) approximation. Full lines represent Greens' functions, while wiggly lines represent the unscreened Coulomb interaction. Double wiggly lines represent the screened interaction whose expansion within the RPA (W_0) is shown on the bottom. Diagrams were drawn using the *feynman* package [230].

practical application of the *GW* approximation feasible, let us first briefly introduce the theory of quasiparticle states and discuss some of their most important properties. For a general introduction to the theory of quasiparticles, see ref. [201]. This discussion closely follows ref. [231] and [127] and the interested reader is referred to those references for more details.

Quasiparticle states provide a rigorous generalization of electronic orbitals to interacting electron systems. Given a complete set of basis functions ψ_i^{QP}, a systems' Greens function can be expressed as

$$G(\mathbf{r},\mathbf{r}';z) = \sum_i \frac{\psi_i^{*QP}(\mathbf{r})\psi_i^{\mathrm{QP}}(\mathbf{r}')}{z-\epsilon_i^{\mathrm{QP}}} \tag{3.32}$$

where i runs over all states, z is a complex number, and ϵ_i^{QP} in the discrete spec-

trum are solutions to the quasiparticle equation

$$\left(\epsilon_i^{\mathrm{QP}} - h_0(\mathbf{r}) - V_H(\mathbf{r})\right)\psi_i^{\mathrm{QP}}(\mathbf{r}) = \int \mathrm{d}\mathbf{r}'\Sigma(\mathbf{r},\mathbf{r}';\epsilon_i^{\mathrm{QP}})\psi_i^{\mathrm{QP}}(\mathbf{r}') \tag{3.33}$$

where $V_H(\mathbf{r})$ is the Hartree potential and h_0 is the non-interacting particle Hamiltonian i.e. $h_0 = T_i + v_{\mathrm{ext}}$ [6]. The eigenvalues to this equation ϵ_i^{QP} have the very nice property that

$$\epsilon_{i-}^{\mathrm{QP}} = E_0^N - E_i^{N-1} \quad \text{if} \quad \epsilon_{i-}^{\mathrm{QP}} < \mu \tag{3.34}$$

$$\epsilon_{i+}^{\mathrm{QP}} = E_i^{N+1} - E_0^N \quad \text{if} \quad \epsilon_{i+}^{\mathrm{QP}} \geq \mu \tag{3.35}$$

where E_0^N, E_0^{N-1}, and E_0^{N+1} are the total ground state energies of the N, $N-1$, and $N+1$ particle system and μ is the chemical potential. The occupied (unoccupied) quasiparticle states therefore describe the addition (removal) of a particle from the N-electron system. For $i = 0$, $\epsilon_{i-}^{\mathrm{QP}}$ and $\epsilon_{i+}^{\mathrm{QP}}$ are equal to the negative ionization potential and electron affinity respectively. The fundamental band gap is accordingly given by:

$$E_{gap} = \epsilon_{0+}^{\mathrm{QP}} - \epsilon_{0-}^{\mathrm{QP}} = E_0^{N+1} + E_0^{N-1} - 2E_0^N \tag{3.36}$$

which is just the same statement as in *Koopmans' theorem* (see section 3.2 Hartree-Fock).

Having briefly discussed some important properties of quasiparticle states, let us now return to the *GW* approximation. We had previously seen, how the *GW* approximation can be physically motivated. Hedin's equations then provide a recipe for finding the quasiparticle wavefunctions and their associated eigenvalues by first

[6] Following ref. [200, 231], here the self-energy corresponds to electron–electron interactions that go beyond the Hartree approximation. This leads to the self-energy (Σ) being a non-local and energy-dependent analogous of the exchange-correlation potential in DFT.

constructing the Green's function and the screened potential from an initial guess, e.g., the results of a mean-field calculation. From this, one can determine Σ as well as a set of new wave functions and energies from eq. (3.33) which in turn leads to the construction of a new Green's function. This procedure can then be iterated until self-consistency is reached. The downside of this approach is that it is rather complicated as the self-energy must be evaluated at the QP energies which are not known *a priori*. Instead, a further simplification is generally introduced which consists in linearizing the QP equation.

Treating the self-energy as a perturbation to the Hamiltonian $H^{\text{eff}} = H_0 + V_{\text{xc}}$[7]. This is justified as long if the initial (DFT) wave functions constitute a good approximation to the true QP wave functions. We can then use perturbation theory in $\Sigma - V_{\text{xc}}$ and to first order write the quasiparticle energies as

$$\epsilon_i^{\text{QP}} = \epsilon_i^{\text{eff}} + Z_i^{\text{eff}} \left\langle \psi_i^{\text{eff}} \middle| \Sigma(\epsilon_i^{\text{eff}}) - V_{\text{xc}} \middle| \psi_i^{\text{eff}} \right\rangle \tag{3.37}$$

where superscripts $^{\text{eff}}$ indicate that the variable corresponds to the effective Hamiltonian (H^{eff}). The renormalization factors Z_i^{eff} are given as

$$Z_i^{\text{eff}} = \left\langle \psi_i^{\text{eff}} \middle| 1 - \Sigma'(\epsilon_i^{\text{eff}}) \middle| \psi_i^{\text{eff}} \right\rangle^{-1} \tag{3.38}$$

and approximate the true QP norm. Here, $\Sigma'(\epsilon_i^{\text{eff}})$ is the derivative of the self-energy with respect to energy as evaluated at the eigenvalues of the effective Hamiltonian (ϵ_i^{eff}).

In principle, this equation can now again be iterated, replacing V_{xc} with the effective self-energy operator $\sum_{i,j} \left|\psi_i^{\text{eff}}\right\rangle \left\langle\psi_i^{\text{eff}}\right| \Sigma(\epsilon_i^{\text{eff}}) \left|\psi_j^{\text{eff}}\right\rangle \left\langle\psi_j^{\text{eff}}\right|$ until self-consistency is reached. This method is known as *quasiparticle self consisted GW* (QPscGW) [232, 233] as opposed to scGW [234] in which the self-energy is calculated for all frequencies and the Green's function is evaluated through the Dyson-Schwinger equation.

[7] Generally, DFT is used as a starting guess for GW calculations.

In practice, it is though much more common to rely on what is called G_0W_0, i.e., a single-shot calculation of the quasiparticle energies starting from DFT results with W_0 being the RPA screened potential (see fig. 3.2). This generally leads to good results at a reasonable computational cost and has become a widely used method in material science.

One of the major disadvantages of the G_0W_0 method is of course its dependency on the DFT starting point with different functionals resulting in notably different quasiparticle energies. A detailed discussion on this can be found in ref. [128, 130, 135]. The success of G_0W_0 is though not only attributable to the high cost of iterative procedures but also the fact that they don't necessarily provide better results. The reason for this lies in the introduction of additional terms in the self-energy which would cancel out in an exact theory e.g. by inclusion of the vertex function which is computationally extremely costly though it results in quasiparticle spectra which are in excellent agreement with experimental data [129, 235, 236]. Another major shortcoming of the G_0W_0 approximation is its inability to describe effects due to electron–hole interaction i.e. excitons (see fig. 3.4). While these effects can to a first approximation be neglected in many cases (particularly in 3D systems), they still play a vital role in determining the optical properties of a number of materials [237] and methods are needed in order to account for them. We will discuss the most common of these methods in the field of solid state physics, i.e. the *Bethe-Salpeter equation* [238–240] (BSE) later in this text.

Before moving on to discussing the BSE method, let us make some final practical remarks regarding the convergence behavior of G_0W_0 calculations with respect to the most important computational parameters.

Just as in "normal" DFT, the result of G_0W_0 calculations depends on a number of computational parameters. The most important ones from a user's point of view are:

- The $\mathbf{q}$-grid used to represent the momentum dependence of the self-energy (Σ) and screened interaction (W). In practical calculations this will be equal to all

possible differences between **k**-points in the irreducible Brillouin zone.

- The energy cut-off (E_{cut}) used in constructing Σ and W (assuming one uses a plane-wave basis).

- The ω-grid used to sample the frequency dependence of Σ and W.

The last of these can be efficiently addressed using a non-linear frequency grid and employing a Hilbert transform as proposed by Shishkin and Kresse [128]. The second problem, i.e., that of convergence with respect to the energy cut-off has been a long-standing issue in *GW* calculations and was first discussed for the case of ZnO by Shih *et al.* [241] and later by Friedrich *et al.* [242] who suggested an empirical $E_{\text{cut}}^{-3/2}$ dependence of the quasiparticle gap. The problem is also encountered for the correlation energies in plane-wave RPA and MP2 calculations, closely paralleling the findings of quantum chemistry, where convergence of the total energies (and excitation energies) with the basis set size is also exceedingly slow. This has long been associated with the description of the interelectron cusp [109, 243–246] which has been found to cause an inverse dependence of the total correlation energy on the number of basis functions (M) [247]. Based on calculations using the Lindhard dielectric function, Kresse and Harl proposed an extrapolation method for the RPA correlation energy, suggesting an asymptotic $1/M$ dependence on the number of basis functions[8] [112]. After Schindlmayr, derived an analytical expression for the *GW* self-energy in a system consisting of two electrons confined on a sphere [248], Klimeš *et al.* demonstrated a more general derivation of the $1/M$ asymptotic behavior of the MP2 and RPA total energies as well as the *GW* self-energy within a plane-wave basis [249]. A result that has been analyzed in detail by Nabok *et al.* [250]. This finally allows one to obtain converged quasiparticle energies by performing a series of calculations at lower energy cut-offs and subsequently extrapolating the

[8] Note that, due to the relationship between energy cut-off and number of plane waves, this is equivalent to the correlation energy depending on $E_{\text{cut}}^{-3/2}$.

individual *GW* self-energies (as well as their derivatives), by exploiting their linear dependence on the inverse number of basis functions in the calculation. Lastly, the issue of slow **q**-grid convergence of the quasiparticle energies is a problem specific to low-dimensional systems. It is caused by the fact that, while in 3D systems, the dielectric function varies only slightly in the region close to $|\mathbf{q}| = 0$, it changes much more drastically in the case of 2D systems [127, 251–255], where screening from the environment is significantly reduced at long wavelengths. Since the Γ-point is always sampled, the screening is typically underestimated causing an overestimation of both, the *GW* quasiparticle corrections and the exciton binding energy (see section 3.7 Bethe-Salpeter Equation), at finite **k**-point samplings. The effect is shown graphically in figure 3.3 via a (non-converged) calculation of the 2D dielectric function of MoS_2 which is defined as [127]

$$\varepsilon_{2D}(\mathbf{q}) = \left[\sum_{\mathbf{G}|\mathbf{G}_{||}=0} e^{iG_z z_0} \varepsilon^{-1}_{\mathbf{G}0}(\mathbf{q}) \right]^{-1} \tag{3.39}$$

The figure shows $\varepsilon_{2D}(\mathbf{q})$ for the MoS_2 monolayer as obtained using both, the bare Coulomb interaction and a 2D-truncated kernel [258]. When using the bare Coulomb interaction, small-**q**, i.e., long-wavelength Coulomb interactions between periodically repeated images along the non-periodic direction are still present resulting in a bulk-like, i.e., slowly changing dielectric function close to $|\mathbf{q}| = 0$. Using a truncated Coulomb interaction on the other hand, all interactions between periodic images along non-periodic directions are avoided, and we see the typical strong **q**-dependence of $\varepsilon_{2D}(\mathbf{q})$ for $|\mathbf{q}| \to 0$. As was already mentioned, it is this strong variation in the dielectric function of 2D materials which causes the slow convergence behavior of *GW* and BSE calculations (see section 3.7 Bethe-Salpeter Equation) for 2D materials with respect to the Brillouin zone sampling as a dense **k**-grid is needed in order to accurately represent the low-**q** variation in $\varepsilon_{2D}(\mathbf{q})$. In order to circumvent this problem, in this work we use the method proposed by Rasmussen *et al.*

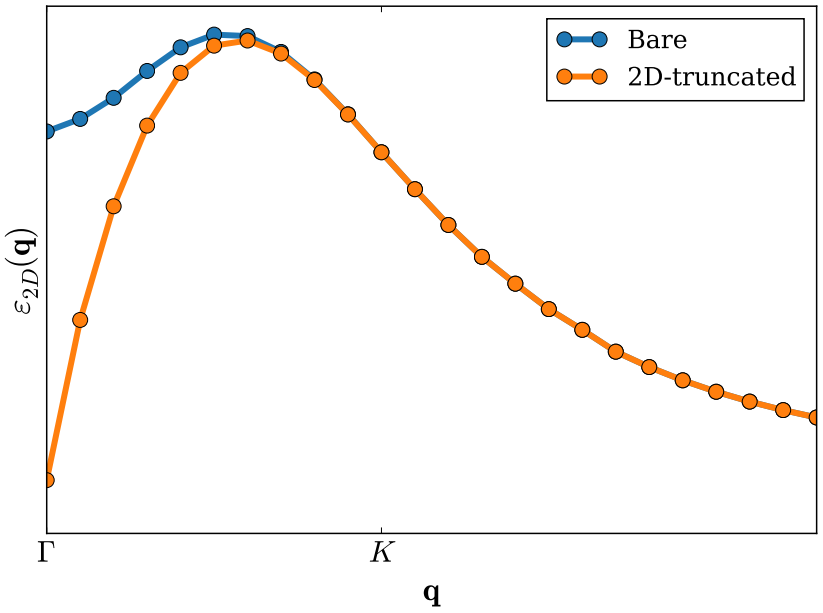

Figure 3.3: 2D static macroscopic dielectric function ($\varepsilon_{2D}(\mathbf{q})$) for MoS_2 using a bare Coulomb interaction and a 2D-truncated kernel. The image was obtained using the GPAW code [256, 257].

[259] and implemented in the GPAW code. It consists in deriving an analytical expression for the small-$|\mathbf{q}|$ limit of the 2D dielectric function which can then be used to integrate the critical area of the 2D Brillouin zone, drastically reducing the needed **k**-point sampling.

The same problem of **k**-grid convergence of course also applies to other calculations involving $\varepsilon_{2D}(\mathbf{q})$, e.g., the BSE method (see section 3.7 Bethe-Salpeter Equation). Unfortunately, there is as of now no version of the aforementioned method available for this type of calculation, thus, dense **k**-grids are required to obtain accurate results.

3.7 Bethe-Salpeter Equation

As was mentioned, one of the major shortcomings of the G_0W_0 method consists in its inability to describe the effects of electron–hole interactions (excitonic effects) on

optical spectra. A schematic representation of the formation of an exciton is shown in fig. 3.4. These interactions play only a minor role in most 3D materials but are much more pronounced in systems of reduced dimensionality due to the decreased screening experienced by the electron–hole pair [132, 253, 260].

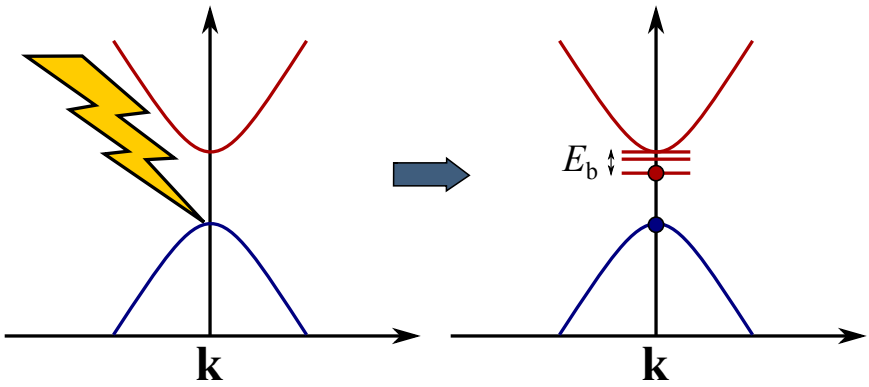

Figure 3.4: Schematic representation of the formation of an exciton which can be viewed as an electron–hole complex, bound by Coulomb interactions. The formation of the exciton results in the formation of states within the band gap region that can be optically active. Here excitonic states are shown as electron states but this is arbitrary and showing them as hole states would be equally valid. E_b indicates the exciton binding energy. The image is adapted from ref. [260].

One way to tackle these issues which is popular in the quantum chemistry community consists in the use of the so-called *configuration interaction singles* (CIS) method which is able to capture excitonic effects starting from a HF or, less commonly, a DFT ground state calculation [152, 261]. While the method has recently been implemented for periodic systems within the CRYSCOR package [125, 126, 262, 263], it still suffers from technical problems such as difficult basis set convergence as well as more fundamental ones, such as its inability to account for screening of the electron–hole interaction by the surrounding medium. A method able to incorporate these effects and which has seen growing popularity in the solid-state community is the so-called Bethe-Salpeter equation or BSE [239]. In the following we will briefly discuss the method, closely following reference [264] (for more details see the review by Onida, Reining and Rubio [238]).

The basic idea of is to reincorporate electron–hole interactions into the polariza-

tion P defined in eq. (3.30). Within G_0W_0, P is approximated by $P = -iGG$. The BSE method now reintroduces the vertex function (Γ) into the equation for P (see (3.30)) thereby reintroducing interactions between electrons and holes. By using the GW expression for the exchange correlation self-energy (Σ^{GW}) and neglecting the variation in the screened Coulomb interaction due to the excitation i.e. the term $\frac{\delta W}{\delta G}$, we can write the vertex as

$$\Gamma(1,2;3) = \delta(1,2)\delta(1,3) + i\int \mathrm{d}(6,7)W(1,2)G(1,6)G(7,2)\Gamma(6,7;3) \tag{3.40}$$

which we can in turn insert into the equation for the polarization in eq. (3.30) i.e.

$$P(1,2) = -i\int \mathrm{d}(3,4)G(2,3)\Gamma(3,4;1)G(4,2) \tag{3.41}$$

giving

$$P(1,2) = -iG(1,2)G(2,1) + \int \mathrm{d}(4,5,6,7)G(1,4)G(5,1)W(4,5)G(4,6)G(7,5)\Gamma(6,7;2) \tag{3.42}$$

If we now define a three-point irreducible polarization as

$$^3P(1,2;3) = -i\int \mathrm{d}(5,6)G(1,5)G(6,2)\Gamma(5,6;3) \tag{3.43}$$

we can write eq. (3.42) as

$$^3P(1,2;3) = -iG(1,3)G(3,2) + i\int \mathrm{d}(4,5)G(1,4)G(5,2)W(4,5)^3P(4,5;3) \tag{3.44}$$

By introducing $L_0(1,2;3,4) = -iG(1,3)G(4,2)$ one can then rewrite the polariza-

tion as a four-point function i.e.

$$^4P(1,2;3,4) = L_0(1,2;3,4) - \int \mathrm{d}(5,6,7,8) L_0(1,2;5,6) W(5,6) \delta(5,7) \delta(6,8) {}^4P(7,8;3,4) \tag{3.45}$$

Lastly we define

$$L(1,2;3,4) =^4 P(1,2;3,4) + \int \mathrm{d}(5,6,7,8) {}^4P(1,2;5,6) {}^4V(5,6,7,8) L(7,8;3,4) \tag{3.46}$$

which when combined with eq. (3.45) gives us the Bethe-Salpeter equation within the *GW* approximation as

$$L(1,2;3,4) = L_0(1,2;3,4) + \int \mathrm{d}(5,6,7,8) L_0(1,2;5,6) K(5,6,7,8) L(7,8;3,4) \tag{3.47}$$

where the kernel K is given by

$$K(1,2;3,4) = V(1,3)\delta(1,2)\delta(3,4) - W(1,2)\delta(1,3)\delta(2,4) \tag{3.48}$$

In practice, eq. (3.47) is solved via the introduction of an effective two-particle Hamiltonian, but this goes beyond the scope of this work and the reader is referred to ref. [264] for details.

3.8 Basis sets and the projector augmented wave method

Having now discussed in some detail the theoretical methods used within this thesis, let us make some short comments as to their implementation, specifically the different types of basis sets used in this work and their individual strengths and weaknesses. We will also briefly discuss the problem of the strongly oscillatory behavior

of the electronic wave function close to the nucleus and how it can be addressed while maintaining access to the all-electron wave function by ways of the projector augmented wave method (PAW) [265].

3.8.1 Basis sets

The term *basis set* within quantum chemistry and computational solid state physics usually refers to the set of functions used to represent the electronic orbitals. While almost any type of function could in principle be chosen for this purpose, it is desirable for practical applications that the basis set fulfill a number of requirements. Some of the most important of which are

1. Eigenvalues of observables (e.g. energy) calculated using the representation of electronic orbitals within the basis set should converge quickly with the size of the basis set, meaning that it should be as *compact* as possible for a given precision.

2. Expectation values of important operators should be easy to calculate. Ideally analytical expressions should be available to evaluate the most important expectation values such as the kinetic energy and the Coulomb interaction.

3. They should allow for a systematic convergence of the wave functions, i.e., one should be able to improve the quality of the basis set in a controlled way towards the complete basis set limit.

Today, there exist many computational chemistry and material science packages employing an array of different basis sets. While it has long been assumed that these different approaches to the electronic structure problem should in principle be convergent to the same results, efforts have only recently been undertaken to test this assumption by systematically probing the reproducibility of computational results using a variety of different programs and basis sets [266]. In this work, we

have employed four different types of basis sets which we will now shortly outline, as well as provide some general comments as to some of their respective strengths and weaknesses.

1. **Linear combination of atomic orbitals (LCAO)** Within the LCAO method, the electronic orbitals are expanded in terms of atomic orbitals. In this work, two different types of such orbitals were used and will be discussed below. Independent of the precise mathematical form of the atomic orbitals used we can though make some general comments as to the strengths and weaknesses of the LCAO approach. Its main advantage is that, since its basis functions closely resemble the atomic orbitals of isolated atoms, they are well suited to describe both valence and core states. They also generally allow to obtain reasonably accurate results using a very compact basis which makes them attractive for use in large systems. The major disadvantages of the LCAO approach lies in the fact that, except for some specifically designed (Gaussian type) sets such as those by Dunning and coworkers [246, 267, 268], Ahlrichs and Weigend [269], Jensen [270–274], or in the periodic case Peintinger and coworkers [275], systematic convergence to the complete basis set limit is difficult and even in the aforementioned cases, steps between different pre-optimized basis sets are rather large. They also suffer from what is known as the BSSE or *basis set superposition error* which expresses the fact that fragments of a system "benefit" from the basis functions located on other parts of the system leading to an artificial lowering of the energy which has to be accounted for in the calculation of, e.g., binding energies. Lastly, while they offer a very cheap and effective description of occupied orbitals, their *localized* nature makes it generally difficult to describe unoccupied states which become increasingly *delocalized* with increasing energy and in the high energy limit where $\langle V \rangle << \langle T \rangle$, that is, the kinetic energy is much greater than the potential energy, are expected to resem-

ble free-electron eigenfunctions.

Let us now discuss the two types of LCAOs used in this work in more detail:

- **Gaussian type LCAOs:** This type of atom-centered basis sets, originally proposed by Preuß [276] and Boys [277, 278], is most common in the quantum chemistry community. The basic idea is to expand orbitals as a linear combination of appropriately optimized Gaussian functions which represent the radial dependence of the basis functions and spherical harmonics which are used to represent their angular dependence. To improve precision, radial functions (called *contracted Gaussian functions*) usually consist of more than one *primitive* Gaussian function. The use of Gaussian functions leads to a number of important expectation values being computable analytically thereby greatly accelerating calculations [279]. The principal reason for the use of Gaussians in quantum chemistry is though what is known as the *Gaussian product theorem*, which states that a product between two Gaussian type orbitals centered on two different atoms can be rewritten as a finite sum of Gaussians centered on a point along the axis connecting them. This leads to the four-center integrals, occurring in the evaluation of e.g. the HF Hamiltonian being reducible to finite sums of two-center integrals, and in a next step to finite sums of one-center integrals. One of the major drawbacks in applying Gaussian type LCAOs in the field of material science is that they do not, in general, form an orthonormal set of functions, leading to linear dependency problems in the overlap matrix which become particularly troubling in periodic calculations [275]. Nowadays, there are many preoptimized basis sets availabe for use. One must thus rarely resort to generating one's own basis sets, making the Gaussian type LCAO approach easy to use even for the layman. Also, while systematic convergence is an issue, extrapolation

schemes towards the full basis set limit exist for both DFT [270–274] and correlation methods [246, 267, 268, 280–286].

- **Numerical LCAOs:** These basis sets differ from the aforementioned Gaussian type LCAOs only in the choice of the radial part of the basis functions. Instead of Gaussians, they are numerically represented on a grid with the angular dependence still represented in terms of spherical harmonics. This approach has the advantage of allowing for more freedom in the functional behavior as it is not limited by the properties of Gaussian functions making it possible to construct basis sets which are even more compact than in the Gaussian case. It also solves the problem of linear dependence in the overlap matrix for periodic calculations as basis functions are usually chosen to have finite support, i.e., each orbital becomes strictly zero beyond some cut-off radius[9]. On of their major disadvantages is that they require numerical procedures for the calculation of expectation values as there exist no analytical expressions as in the case of Gaussian type orbitals. Other than this, they share most of the advantages and disadvantages of Gaussian type LCAOs including BSSE.

2. **Plane waves (PW):** As we have seen, LCAO type basis sets conceptually start from an atomic description of the system, appropriately adding functions to better account for the change in electron-distribution due to the formation of chemical bonds in a molecule and/or solid. Plane wave basis sets on the other hand take what might be conceived as the opposite approach, starting from a *free electron like* description and expanding atomic states as a linear combination of free electron eigenfunctions. While this has the advantage of leading to an excellent description of highly *delocalized* electronic situations e.g. valence electrons in metals, the method naturally struggles to describe strongly *localized*

[9] See the Siesta [287, 288] user's manual for details [289].

electrons close to the atomic nuclei . The reason for this is that the expansion coefficients of the electronic orbitals in a plane wave basis are nothing but the coefficients of its Fourier transform which converges only slowly for quickly-varying functions. The advantages of the method is that the size of the basis set can be very easily controlled by a single parameter, the so-called *energy cut-off* (E_{cut}) facilitating systematic convergence of the results. Basis functions are also themselves eigenfunctions to the kinetic energy operator making its evaluation trivial. As mentioned previously, high-lying unoccupied states of any system are expected to resemble free electron like states and the basis set therefore naturally lends itself to the derivation of extrapolation schemes as we have seen in the case of RPA, *GW* and MP2. Lastly, the basis set is independent of the atomic positions making it easy to evaluate forces using the Hellmann-Feynman theorem [290, 291] and also causing the method to be free of BSSE. Disadvantages lie in the aforementioned difficulty in describing quickly-varying functions making the description of electrons close to the atomic nuclei challenging and requiring in general the use of pseudopotentials and/or auxiliary basis sets [292]. Also, while the basis set is independent of the atomic positions, it does depend on the size of the unit cell used in the calculation, thereby causing artifacts in volume relaxations if the cut-off value is not sufficiently converged. This phenomenon is known as *Pulay stress* [293]. Plane wave basis sets are also in general far less compact than LCAO ones as vacuum regions surrounding non-3D systems i.e. slabs (2D), rods (1D) or molecules (0D), require the same amount of basis functions as do the more chemically relevant (at least for ground-state calculations) regions of space occupied by atoms. Further, due to the nature of the plane wave basis functions as being infinitely extended in three-dimensions, plane wave calculations necessarily require periodic boundary conditions to be applied along all spacial directions meaning that systems have to be surrounded by large amounts of vacuum to isolate them from their

periodic images along non-periodic directions. Lastly, while the kinetic energy operator can be efficiently evaluated in reciprocal space, the evaluation of the exchange-correlation potential is performed in real space. Fourier transformations to and from real space must therefore be carried out during each self-consisted-field cycle. As these are inherently non-local operations, they can cause problems with scalability in highly-parallel applications and render the development of order-N methods difficult [257].

3. **Real-space grids (FD):** Real-space grids (or finite difference methods) represent what may be the simplest among all the approaches discussed here. In these methods, no basis set is actually used and electronic orbitals are represented at a series of points distributed either regularly or irregularly throughout the computational cell [256, 257, 294]. All expectation values are computed using finite-difference methods with the accuracy of the operations depending on the density of points as well as the finite-difference stencil used. The method shares many of the advantages and disadvantages of the plane-wave expansion. The main differences lying in their parallelizability, which is better in the case of FD, and the ease of evaluation of operators, which is worse in the case of FD as all operations have to be performed numerically. A grid-based representation of the orbitals also leads to a rather large memory footprint which can though be overcome in part by parallelization over real-space domains (see citations [256] and [257] as well as citations therein for details). On the other hand, the method has the advantage of not imposing specific requirements on the periodic boundary conditions of the system (as is the case, e.g., for PW which always requires a 3D-periodic cell) allowing for the calculation of 0D-3D periodic systems on the same theoretical footing.

3.8.2 The Projector augmented wave method

As mentioned before, one of the major challenges for many types of basis sets used in periodic calculations lies in the description of the quickly-varying electronic orbitals close to the atomic nuclei which makes it necessary to use large numbers of plane waves, or equivalently very fine grid spacings, thereby significantly increasing the cost of the calculations. Given that one is generally more interested in the behavior of electrons *away* from the atomic nuclei, i.e., the *valence* region which largely determines the chemical properties of a system, it would be highly desirable to avoid spending large amounts of resources on the description of the chemically largely irrelevant core-region. One way to overcome this problem is via the use of so-called *pseudopotentials* (see ref. [295] and references therein), which were originally introduced by Hellman in 1935 [296] and which substitute the true atomic potential by a smoother *effective* potential [297–302]. Pseudopotentials significantly lower the number of orbitals to be calculated, since the pseudopotentials only have to be calculated and tabulated once for a given type of atom, thereby effectively removing the core electrons from the calculation. The major disadvantage of this method is that the removal of core electrons from the calculations makes it impossible to gain any information on the full electronic wave function. While this might seem unimportant in many cases it has been shown by Kresse *et al.* to strongly influence the result of *GW* calculations, where a LDA-level treatment of core-valence interactions results in an error in the quasiparticle energies of up to 0.1–0.2 eV [128] as compared to the more accurate HF treatment. The latter is though not possible within the pseudopotential approximation as the charge distribution and the electronic orbitals of valence electrons in the core region are not physically meaningful [128, 303]. An alternative to the use of pseudopotentials which solves many of the problems associated with them was proposed by Blöchl in 1994 [265] and is known as the *projector augmented wave method* (PAW). In the following, we will briefly lay out some basic ideas and

features of the PAW method, whereby we closely follow ref. [304].

As a first step, let us define an auxiliary smooth (and thereby computationally efficient) electronic orbital $|\tilde{\psi}_n\rangle$ which is related to the true all electron orbital $|\psi_n\rangle$ as

$$|\tilde{\psi}_n\rangle = \mathcal{T}\,|\psi_n\rangle \tag{3.49}$$

The true orbitals are already smooth outside of the aforementioned small regions around the atomic nuclei, i.e., $|\tilde{\psi}_n\rangle = |\psi_n\rangle$ for $|\mathbf{r} - \mathbf{R}_a| > r_c^{(a)}$ with $r_c^{(a)}$ the cut-off radius for the augmentation region. $\mathcal{T}$ should therefore only modify the orbitals within those regions. We can thus define the total transformation operator $\mathcal{T}$ as a sum over atom-centered transformations $\mathcal{T}^{(a)}$ with a the index of the atom. This leads us to the definition

$$\mathcal{T} = 1 + \sum_a \mathcal{T}^{(a)} \tag{3.50}$$

where every $\mathcal{T}^{(a)}$ is zero outside of the sphere of radius $r_c^{(a)}$ around atom a. Inside the augmentation regions, we can expand the true all electron orbitals ($|\psi_n\rangle$) in terms of partial waves $\left|\phi_i^{(a)}\right\rangle$. For each of these partial waves, we define a corresponding auxiliary smooth partial wave $\left|\tilde{\phi}_i^{(a)}\right\rangle$ and require that

$$\left|\phi_i^{(a)}\right\rangle = \left(1 + \mathcal{T}^{(a)}\right)\left|\tilde{\phi}_i^{(a)}\right\rangle \tag{3.51}$$

for all i and a which completely defines $\mathcal{T}$ given $|\phi\rangle$ and $|\tilde{\phi}\rangle$. If the smooth partial waves form a complete set inside the augmentation sphere of atom a, we can expand the smooth all electron orbitals around that same atom as

$$|\tilde{\psi}_n\rangle = \sum_i \left\langle \tilde{p}_i^{(a)} \middle| \tilde{\psi}_n \right\rangle \left|\tilde{\phi}_i^{(a)}\right\rangle \tag{3.52}$$

for $|\mathbf{r} - \mathbf{R}_a| > r_c^{(a)}$, where and $\left|\tilde{p}_i^{(a)}\right\rangle$ are some fixed functions termed *smooth pro-*

jector functions and which, assuming there to be no overlap between augmentation spheres, together with the smooth partial waves satisfy

$$\sum_i \left|\tilde{\phi}_i^{(a)}\right\rangle \left\langle \tilde{p}_i^{(a)}\right| = 1 \tag{3.53}$$

inside each augmentation sphere. With this, we can now write down an explicit definition of our projection operator $\mathcal{T}$ as

$$\mathcal{T} = 1 + \sum_a \sum_i \left(\left|\tilde{\phi}_i^{(a)}\right\rangle - \left|\phi_i^{(a)}\right\rangle\right) \left\langle \tilde{p}_i^{(a)}\right| \tag{3.54}$$

This means the all electron orbitals can be expressed as

$$|\psi_n\rangle = |\tilde{\psi}_n\rangle + \sum_a \sum_i \left(\left|\tilde{\phi}_i^{(a)}\right\rangle - \left|\phi_i^{(a)}\right\rangle\right) \left\langle \tilde{p}_i^{(a)} \middle| \tilde{\psi}_n\right\rangle \tag{3.55}$$

A graphical representation of the resulting decomposition for the case of LiH is shown in fig. 3.5.

So, what have we achieved by this transformation? Our initial problem was that the all-electron orbitals display rapid oscillations in some parts of space while behaving smoothly in other parts. Decomposition (3.55) now allows us to express the all-electron orbitals in terms of computationally convenient smooth auxiliary orbitals. The remaining atomic terms are localized within well-defined augmentation spheres around the individual atoms and can be effectively represented on atom centered radial grids.

It is important to stress that decomposition (3.55) can in principle be made *exact* and does not in and of itself represent an approximation. Any practical application of the PAW method does though generally involve a series of approximations such as

- Using only a finite number of partial waves (and thereby smooth partial waves and projector functions).

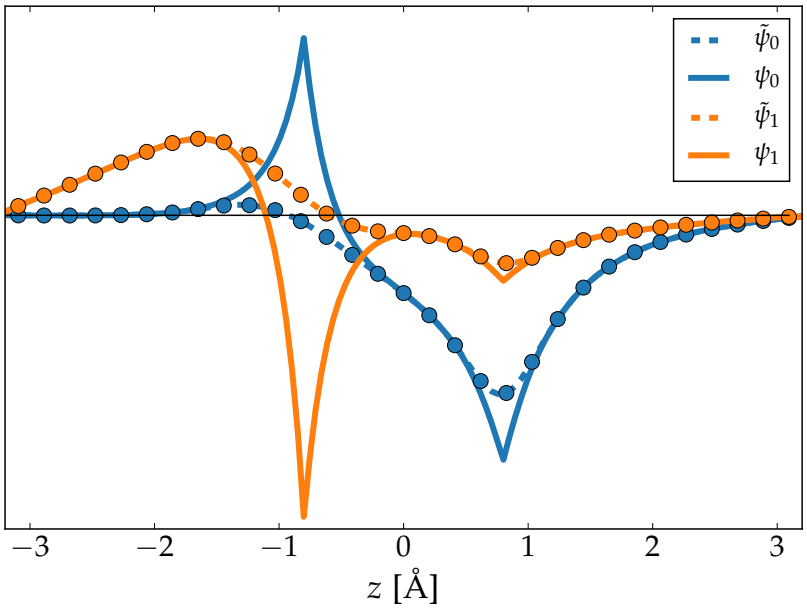

Figure 3.5: All electron $(\psi_{1/2})$ as well as smooth pseudo orbitals $(\tilde{\psi}_{1/2})$ as defined in eq. (3.55) plotted along the molecular axis (z) of LiH . The image was obtained using the GPAW code.

- The frozen core approximation, i.e., assuming $|\psi_n^{\text{core}}\rangle = |\chi_\alpha^{a,\text{core}}\rangle$, where n refers to both a specific atom and a specific atomic state. For an evaluation of the frozen core approximation within PAW, see ref. [305].

- Possible overlap between the augmentation spheres.

Though these approximations introduce some small errors into the calculation, the PAW method still allows all electron calculations within the frozen core approximation to be performed at the same cost as calculations involving pseudopotentials and has become widely used in solid state physics with a number of codes implementing its use [145, 256, 257, 306–312].

3.9 Non-equilibrium Green's functions

While there are a number of ways to address the problem of electronic conductance from a computational chemist's point of view, the method employed in this work consists in the use of non-equilibrium Green's functions. In the following we will show how, within this scheme, the equation for the steady-state current through a device (scattering region) can be derived. Herein we will closely follow ref. [313].

The computational model used for this type of process consists of three parts, i.e., a central scattering region (device) which is connected to two semi-infinite leads connecting the scattering region to the two reservoirs at their respective chemical potentials ($\mu_{1/2}$). Assuming there to be no interaction between the two leads, the total Hamiltonian of the system can then be written as follows

$$H = \begin{pmatrix} H_1 & \tau_1 & 0 \\ \tau_1^\dagger & H_{\text{scat}} & \tau_2^\dagger \\ 0 & \tau_2 & H_2 \end{pmatrix} \tag{3.56}$$

with H_1 and H_2 the Hamiltonians of the two semi-infinite leads, H_{scat} the Hamiltonian of the scattering region and $\tau_{1/2}$ describing the coupling of the scattering region to the leads. Using the basic properties of Green's functions one is now able to write the Green's function, of the scattering region (G_{scat}) under the influence of the two semi-infinite leads as

$$G_{\text{scat}} = (E - H_{\text{scat}} - \Sigma_1 - \Sigma_2)^{-1} \tag{3.57}$$

where Σ_1 and Σ_2 are the self-energies for the two semi-infinite leads. Equation (3.57) nicely illustrates the reason for using Green's functions rather than attempting a direct solution of the problem starting from its electronic Schrödinger equation. While the latter requires the solution of the complex three-component problem (leads plus scattering region), the former allows us to separate it into three subproblems

which are considerably easier to solve. The solutions for the entire system can then be obtained from the rather simple coupling shown in eq. (3.57).

In the non-equilibrium case, reservoirs at different chemical potentials will inject electrons into the states corresponding to incoming waves in the contacts. Considering contact 1, let us denote those wave functions which in the isolated contact are being completely reflected at the end of the contact as $|\psi_{1,n}\rangle$, where n indexes all possible solutions of this type. We can now write the device and lead wave functions caused by the incoming wave in contact 1 as

$$|\psi_{\text{scat}}\rangle = G_{\text{scat}}\tau_1^\dagger |\psi_{1,n}\rangle \tag{3.58}$$

$$|\psi_1\rangle = \left(1 + g_1\tau_1 G_{\text{scat}}\tau_1^\dagger\right) |\psi_{1,n}\rangle \tag{3.59}$$

$$|\psi_2\rangle = g_2\tau_2 G_{\text{scat}}\tau_1^\dagger |\psi_{1,n}\rangle \tag{3.60}$$

where $g_{1/2}$ are the Green's functions for the isolated leads 1 and 2 respectively and G_{scat} is the scattering region Green's function.

These results can now be used to compute the properties of the combined system (leads + scattering region). Herein we will exclusively discuss the computation of the current traversing a device and the reader is referred to the literature for a description of other properties that can be obtained from the method [313–317]. In order to derive the desired expression for the current we make use of the continuity equation and the fact that in the steady-state, the probability to find an electron on the device is constant in time i.e.

$$\frac{\partial\left(\sum_i |\langle\psi|\, i\rangle|^2\right)}{\partial t} = 0 \tag{3.61}$$

where the sum is taken over scattering region eigenfunctions ($|i\rangle$). Rearranging the terms in eq. (3.61) we can write it as

$$\frac{\partial \sum_i |\langle \psi | i \rangle|^2}{\partial t} = \sum_i \left(\frac{\partial \langle \psi | i \rangle}{\partial t} \langle i | \psi \rangle + \langle \psi | i \rangle \frac{\partial \langle i | \psi \rangle}{\partial t} \right) \tag{3.62}$$

$$= \frac{i}{\hbar} \sum_i \left[\langle \psi | H | i \rangle \langle i | \psi \rangle - \langle \psi | i \rangle \langle i | H | \psi \rangle \right] \tag{3.63}$$

Using the decomposition of H shown in eq. (3.56) and resolving the sums $(\sum_i |i\rangle \langle i| \psi\rangle = |\psi_{\text{scat}}\rangle)$, (3.63) can be rewritten as

$$\frac{i}{\hbar} \left[\langle \psi | H_{\text{scat}} + \tau_1 + \tau_2 | \psi_{\text{scat}} \rangle + \langle \psi_{\text{scat}} | H_{\text{scat}} + \tau_1^\dagger + \tau_2^\dagger | \psi \rangle \right] \tag{3.64}$$

$$= \frac{i}{\hbar} \left[\langle \psi_1 | \tau_1 | \psi_{\text{scat}} \rangle - \langle \psi_{\text{scat}} | \tau_1^\dagger | \psi_1 \rangle \right] + \frac{i}{\hbar} \left[\langle \psi_2 | \tau_2 | \psi_{\text{scat}} \rangle - \langle \psi_{\text{scat}} | \tau_2^\dagger | \psi_2 \rangle \right] \tag{3.65}$$

Let us briefly discuss the last of these equations: We can identify the first term as representing the probability current entering the device from lead 1, while the second term represents the current coming from lead 2. This means that the probability current due to an arbitrary contact (I_j) can be written as

$$I_j = \frac{i}{\hbar} \left[\langle \psi_j | \tau_j | \psi_{\text{scat}} \rangle - \langle \psi_{\text{scat}} | \tau_j^\dagger | \psi_j \rangle \right] \tag{3.66}$$

In order to compute the total probability current through the device we now simply insert the definitions of $|\psi_{\text{scat}}\rangle$, $|\psi_1\rangle$ and $|\psi_1\rangle$ from eq. (3.60). This gives the probability current into the device, caused by and incoming wave from lead 1 ($|\psi_{1,n}\rangle$) through the coupling defined by τ_2 as

$$I_2 = \frac{i}{\hbar} \left[\langle \psi_2 | \tau_2 | \psi_{\text{scat}} \rangle - \langle \psi_{\text{scat}} | \tau_2^\dagger | \psi_2 \rangle \right] \tag{3.67}$$

which, after some algebra gives

$$I_2 = \frac{i}{\hbar} \langle \psi_{1,n} | \tau_1 G_{\text{scat}}^\dagger \tau_2^\dagger \left(g_2^\dagger - g_2 \right) \tau_2 G_{\text{scat}} \tau_1^\dagger | \psi_{1,n} \rangle \tag{3.68}$$

Summing over all n and noting that electrons are entering contact 1 from reservoir 1 at a chemical potential μ_1 and with the Fermi-Dirac distribution $f(E, \mu_1)$, we obtain

$$I_2 = -2\frac{\pi}{h}\int_{-\infty}^{\infty} \mathrm{d}E f(E, \mu_1)\mathrm{Tr}\left[G^{\dagger}_{\mathrm{scat}}\Gamma_2 G_{\mathrm{scat}}\Gamma_1\right] \tag{3.69}$$

where the factor 2 accounts for spin-degeneracy and we have defined the spectral broadening matrix $\Gamma_i = i\tau_i^{\dagger}\left(g_i^{\dagger} - g_i\right)\tau_i$.

Finally, we subtract the probability current from lead 2 to obtain the well-known Landauer formula for the probability current

$$I = -2\frac{\pi}{h}\int_{-\infty}^{\infty} \mathrm{d}E \left(f(E, \mu_1) - f(E, \mu_2)\right) T \tag{3.70}$$

with the transmission T defined as

$$T = \mathrm{Tr}\left[G^{\dagger}_{\mathrm{scat}}\Gamma_2 G_{\mathrm{scat}}\Gamma_1\right] \tag{3.71}$$

Chapter 4

Results

M1: Strong 1D localization and highly anisotropic electron-hole masses in heavy-halogen functionalized graphenes

L. E. Marsoner Steinkasserer, A. Zarantonello, and B. Paulus

Phys. Chem. Chem. Phys. **18**, 36, 25629-25636 (2016)

DOI: 10.1039/C6CP05188J

URL: http://dx.doi.org/10.1039/C6CP05188J

Author contributions

The project was initially conceived by myself. Alessandra Zarantonello performed initial test calculations and explored various possible alternative directions for the project. All calculations contained in the manuscript were performed by myself. Kirsten Trøstrup Winther and Filip Anselm Rasmussen provided the latest development version of the GPAW-GW code as well as help with its proper use. Thomas Olsen helped with the use of the GPAW BSE module as well as making general suggestions as to the technical setup of the BSE calculations. Johannes Voss suggested studying the effect of Br–Br buckling and thereby the use of the 2×1 supercell construction. Jean Christophe Tremblay helped in formulating the discussion of possible effects of the effective mass asymmetry on exciton-recombination while Johannes Horst Budau, Gunter Hermann, Vincent Pohl and Marcel Quennet all made general

suggestions and gave feedback on the work. Writing of the manuscript was done by myself in collaboration with Beate Paulus. Alessandra Zarantonello provided helpful criticism and suggestions as to its improvement.

M2: Cyanographone and Isocyanographone – two asymmetrically functionalized graphene pseudohalides and their potential use in chemical sensing

L. E. Marsoner Steinkasserer and B. Paulus

ArXiv preprint arXiv:1703.08582 (2017)

URL: http://arxiv.org/abs/1703.08582

Author contributions

The project was initially conceived by myself. All calculations in the manuscript were performed by myself with Vincent Pohl helping with the use of the ASE transport module. Ask Hjorth Larsen provided helpful discussion on the libvdwxc implementation of the vdW-DF-CX functional.

The manuscript was written by myself in collaboration with Beate Paulus. Carmen Reden helped in proofreading the manuscript.

M3: Hybrid density functional calculations of the surface electronic structure of GdN

L. E. Marsoner Steinkasserer, B. Paulus, and N. Gaston

Phys. Rev. B **91**, 23, 235148 (2015)

DOI: 10.1103/PhysRevB.91.235148

URL: http://dx.doi.org/10.1103/PhysRevB.91.235148

Author contributions

The project was initially conceived by Nicola Gaston and myself. All calculations were performed by myself with input from Nicola Gaston. Marcel Quennet helped with the discussion of some of the computational aspects of the project.

The manuscript was written by myself in collaboration with Beate Paulus, Nicola Gaston. Both Franck Natali and Joe Trodahl provided helpful feedback and criticism.

M4: Structural and electronic properties of graphene nanoflakes on Au (111) and Ag (111)

J. Tesch, P. Leicht, F. Blumenschein, L. Gragnaniello, M. Fonin, L. E. Marsoner Steinkasserer, B. Paulus, E. Voloshina, and Y. Dedkov

Sci. Rep. **6**, 23439 (2016)

DOI: 10.1038/srep23439

URL: http://dx.doi.org/10.1038/srep23439

Author contributions

The project was initially conceived by Beate Paulus, Mikhail Fonin, Elena Voloshina and Yuriy Dedkov. Experiments were performed by Mikhail Fonin, Julia Tesch, Philipp Leicht, Felix Blumenschein, and Luca Gragnaniello while Elena Voloshina and myself performed the DFT calculations in close collaboration with Beate Paulus.

The manuscript was written by Julia Tesch, Mikhail Fonin, Elena Voloshina and Yuriy Dedkov with input from myself.

M5: Weak interactions in Graphane/BN systems under static electric fields - A periodic ab-initio study

L. E. Marsoner Steinkasserer, N. Gaston, and B. Paulus

J. Chem. Phys. **142**, 15, 154701 (2015)

DOI: 10.1063/1.4917170

URL: http://dx.doi.org/10.1063/1.4917170

Author contributions

The initial idea for the project was formulated by myself and I performed all calculations in the manuscript. Beate Paulus suggested the study of the effect of external fields on the band structure as well as the calculation of dipole moments and polarizabilities, leading to a complete reworking of the manuscript and refocusing of the project. Lukas Hammerschmidt helped with the use of the CRYSCOR code while Andreas Achazi made suggestions as to the design of the appropriate basis set. The manuscript was written by myself in collaboration with Beate Paulus and Nicola Gaston.

M6: Band-gap control in phosphorene/BN structures from first-principles calculations

L. E. Marsoner Steinkasserer, S. Suhr, and B. Paulus

Phys. Rev. B **94**, 125444 (2016)

DOI: 10.1103/PhysRevB.94.125444

URL: http://dx.doi.org/10.1103/PhysRevB.94.125444

Author contributions

The project was initially conceived by myself and all calculations were performed by myself. Simon Suhr performed initial tests and explored various possible alternative directions for the project. The finial form of the project was formulated by Beate Paulus and myself. Kirsten Trøstrup Winther and Filip Anselm Rasmussen provided the latest development version of the GPAW-GW code and made helpful suggestions as to its proper use. The manuscript was written by myself in collaboration with Beate Paulus. Simon Suhr, Lukas Hammerschmidt, Carmen Reden, and Lisa Suntrup all helped in proofreading the manuscript.

Chapter 5

Summary

The aim of this thesis was twofold: firstly, using model many-body methods to explore the properties of known vdWHs and elucidate the role and delicate interplay of different types of interactions on their properties; secondly, using those same methods to explore new types of materials based on the chemical functionalization of graphene.

With the range of experimentally accessible graphene derivatives quickly expanding, the future of functionalized graphenes seems bright. Challenges though still remain as known structures struggle to meet the requirements set by many of the most important fields of application. While e.g. ideal photovoltaic materials should possess an electronic band gap of $\approx 0.9 - 1.6$ eV [318], graphane and fluorographene both show significantly greater band gaps around 3.8 eV [319], much too large for use in solar cells. A possible remedy for this problem consists in the introduction of heavier halogen atoms into these structures. As those are more polarizable than their lighter counterparts, they could lead to a significant reduction in the band gap while at the same time maintaining halogenated graphenes' major advantages over other 2D materials such as their environmental stability and not having to use rare elements in their synthesis. A significant step in this direction was made by František Karlický and coworkers when they performed a systematic study on the properties of **halogenated graphenes** of varying stoichiometry [71]. They

identified two materials with the chemical composition C_2FBr and C_2HBr, which not only seemed to be thermodynamically stable but also showed band gaps close to the ideal values for use in solar cells. Motivated by these initial results, I decided to perform an in-depth investigation into the materials' properties using modern many-body electronic structure techniques. I further extended on the materials originally proposed by Karlický *et al.* by studying the effect of asymmetric functionalization (see paper M1). Using more sophisticated techniques I was able to confirm the findings of Karlický *et al.*, showing fully or partially brominated fluorographene derivatives to posses optical gaps within the ideal range for use in solar cells. This study also revealed another fascinating property of these materials: While the lowest-lying conduction bands were found to be largely *delocalized* over the entire 2D layer, the highest-energy valence bands were strongly *localized* along the rows of bromine/chlorine atoms, resulting in a strong asymmetry in the charge carrier effective masses. While electrons are free to move within the 2D layer, holes are heavily constrained to only move along the chains of bromine/chlorine atoms. This behavior is not only interesting on theoretical grounds but could potentially be exploited to improve the materials' quantum efficiency. The strongly asymmetric effective masses lead to electrons, upon excitation of the material, quickly diffusing over the 2D layer. Holes on the other hand are highly constrained along one of the two spatial directions. This causes quick decay in the overlap between the electron and hole wave functions, which in turn could significantly suppress recombination rates of excited electron–hole pairs though more detailed investigations are of course needed to verify whether this is indeed the case. The study finally resulted in the publication of paper M1.

The fascinating and unexpected properties of brominated graphenes motivated me to consider other, as of now un- or underexplored, graphene derivatives. Again starting from the work of František Karlický and coworkers I decided to investigate the properties of graphene pseudohalides, specifically cyano- and isocyanographenes.

Even before their first experimental realization, which came only towards the end of my study, these materials had been proposed as potentially potent gas sensors [67]. While fully functionalized cyano- and isocyanographene show band gaps close to those of graphane and fluorographene, half-functionalization on only one of the two graphene faces results in materials which are conducting at room temperature. In analogy to half-functionalized graphane (graphone) I use the suffix *-one* to refer to these materials, calling them **cyano- and isocyanographone** respectively. Though asymmetric functionalization alleviates the band gap issue, it potentially introduces a new problem as e.g. graphone has long been known to suffer from low thermal stability [320]. One solution to this issue that has been proposed by Hemmatiyan *et al.* is to adsorb graphone on BN [88, 321]. This not only significantly increases its stability, but also makes its synthesis potentially much easier as BN polarizes the adsorbed graphene layer. Using the same approach, I was able to show that the stability of both cyano- and isocyanographone can be significantly enhanced by BN adsorption. In the case of isocyanographone, this stabilization leads to it changing from only being kinetically stable to being thermodynamically stable with respect to decomposition. Given these promising results, I then employed non-equilibrium Green's function theory [313–317] to study the changes in the transport properties of BN-adsorbed cyanographone (GrCN@BN) upon adsorption of N_2, O_2, CO_2 and CO. I found that, while N_2, O_2 and CO_2 adsorption has little to no influence on the GrCN@BN $I-V$ curves, CO adsorption leads to a reduction in the current to $\approx 40\%$ of its value in the pristine system over a range of tested voltages. Together with the experimental advancements in cyanographene synthesis, these results lend further support to the proposition of using cyanographone as a gas sensing material with a potentially broad range of applications. The results of this work were recently published on the ArXiv (paper M2).

The study on cyano- and isocyanographone largely focused on the former's more stable BN-adsorbed form which does not display any type of long-range magnetic

ordering. Both the isolated cyano- as well as isocyanographone layer though, do show ferromagnetic ground states which can be attributed to the presence of an unpaired electron on one of the two graphene sublattices. As in the case of graphone [32, 88, 320, 322–329] this makes the material potentially applicable to use in spintronics. While as of now, no further investigated the magnetic properties of pristine cyano- and isocyanographone were undertaken, I have, as part of my stay at the Victoria University of Wellington, worked on another type of magnetic material, namely **Gadolinium nitride (GdN)**. The study was motivated by the work of Joe Trodahl and Franck Natali (both at Victoria University) who had performed extensive research on the properties and potential use of rare-earth mononitrides in spintronics. Among these materials, GdN is of particular interest as it possesses an extremely large magnetic moment, caused by the 7 unpaired electrons in its half-filled f-shell, while at the same time displaying a band gap which puts it into the class of ferromagnetic semiconductors. In my work I analyzed the differences in the electronic structure of GdN bulk and its (111) surface. Given the strong interaction between same-spin electrons present in the Gd^{3+} half-filled f-shell, an appropriate description of these systems requires the use of hybrid functionals. Using the HSE06 functional, I was able to not only demonstrate the appearance of metallic surface states in the majority-spin channel upon creation of the (111) surface from the GdN bulk structure, but also the formation of a minority-spin electron-pocket, localized within the bulk region of the computational slab model. Additionally, for the case of bulk GdN, I analyzed the dependence of the direct and indirect band gap as well as the average position of the occupied f-manifold on the fraction of short-range HF exchange included within the HSE-type functional. The resulting linear relationships might well be used to construct an *optimized* HSE-type functional for the study of different GdN systems in the future. The results of this work have been published in paper M3.

Aside from the study of what might loosely be called *strongly bound materials*, i.e.

chemically modified graphenes and GdN, the second central subject of my thesis concerned the study of weakly interacting, multilayered structures, so-called *van der Waals heterostructures* (vdW-heterostructures). Interest in these has grown tremendously over recent years as they show a number fascinating properties such as the presence of interlayer excitons [84–87] with potentially wide-ranging applications. More crucially they allow for a complete rethinking of atomic-scale material science in terms of a set of fundamental building blocks (the 2D layers) which can be freely combined into arbitrarily complex structures in a manner not dissimilar to the assembly of Lego blocks [82]. Tough the weak interaction between these individual layers is what allows for them to be so freely combinable, they can nonetheless significantly impact the heterostructure's properties, allowing for the possibility of custom-designing materials for a specific application. From a theoretical point of view, these systems are no less fascinating as the weak interactions which so strongly determine their properties are due to long-range electron correlation. While an *ab-initio* treatment of these effects requires the application of computationally demanding many-body electronic structure theory, there exist a number of methods which allow for their approximate description within the confines of standard DFT, some of which were used in this thesis [92–101, 189]. My initial work on the subject, which was conducted in close collaboration with Elena Voloshina, focused on the effects of metal (specifically gold and silver) deposition on the properties of **graphene nanoflakes** – in particular their doping levels and changes in the graphene Fermi velocity. While these systems can not be strictly considered as being vdW-heterostructures, given that the gold/silver substrate is not made up from weakly interacting layers, the interaction between the substrate and the graphene monolayer shares all the important properties of vdW-heterostructures such as the relative weakness of the interaction as well as the importance of the support in determining the properties of the adsorbed material. The project was a joint collaboration with the experimental group of Mikhail Fonin from the Universität Konstanz and finally resulted in the

publication of paper M4. Apart from providing further insight into the properties of graphene/metal interfaces, it also clearly demonstrated some of the limitations of the semi-empirical methods used to account for vdW-interactions. Tough agreement with experimental results was very good in general, the two methods used, namely Grimme's DFT-D2 [92] and DFT-D3 [93, 94] approach, showed somewhat disagreeing results with regards to the doping levels of gold and silver adsorbed graphene. While DFT-D2 better reproduced experimental results in the case of silver adsorbed graphene, DFT-D3 seemingly performed better for the gold adsorbed graphene while slightly larger disagreement with the experimental data was found for silver.

These findings, together with a paper by Jukka T. Tanskanen and coworkers [330], in which they studied graphane-type systems using *ab-initio* LMP2 calculations, lead me to the study of **graphane/BN heterostructures**. While these systems share the computationally demanding, delicate interplay of mean-field interactions and electron correlation effects of other vdW-heterostructures, their large band gaps and relatively simple electronic structure make them an ideal case study for the use of *ab initio* approaches in periodic systems. The study itself was performed at the University of Wellington (NZ) in collaboration with Nicola Gaston (formerly of Victoria University of Wellington, now University of Auckland). Using the aforementioned LMP2 method as implemented in the CRYSCOR code [124–126] I was able to show that, while the binding between graphane and BN is purely due to vdW-interactions, the preference of graphane for a particular BN adsorption site is instead dictated by mean-field, i.e., HF-level repulsion between the two layers, with the strength of electron correlation effects, that is the magnitude of the LMP2 corrections to the HF interaction energy, being largely independent of the relative position of the two layers. Given that many of the proposed applications for 2D systems consist in their use within electronic circuits, I subsequently decided to investigate the effects of applying external electric fields to the graphane/BN multilayers. As a first step, again

using the LMP2 method, I calculated both dipole moments and polarizabilities along the surface normal direction for mono-, bi- and trilayer systems. While I found the inclusion of electron correlation to only weakly affect static response properties, this still represented the, to the best of my knowledge, first calculation of *ab initio* polarizabilities for periodic systems. Finally turning to the systems electronic band structure, I demonstrated drastic changes in its quantitative and qualitative features under the effect of external electric fields. I found that the BN bands in particular were highly sensitive to the external field and could be strongly shifted in energy. Depending on the field direction and strength, the band gap was altered significantly in size and in the case of BN/graphane/BN the external field could be used to selectively induce charge transfer from the graphane to one of the two BN layers. The results of this study were finally published in paper M5.

Building on these results as well as previous experience with the *GW* method [200, 225, 227], I decided to turn my attention towards another type of 2D material by investigating the effects of BN-adsorption on the electronic properties of **phosphorene** [30–37], a 2D form of black phosphorus that had only recently been isolated for the first time. Phosphorene is a close to ideal material for this type of study. It possesses an optical gap of $\approx 1.3 - 1.75$ eV [331–334] which is close to the optimal value for use in solar cells [318]. The material further shows anisotropic electronic, mechanical, optoelectronic, and thermo-electric properties, which render it an interesting system for a number of potential applications [335]. Complicating its practical use though, is the low environmental stability of phosphorene as it has been found to quickly degrade upon exposure to oxygen under ambient conditions [336]. One possible way to circumvent this problem, while at the same time maintaining phosphorene's many attractive properties, consists in its encapsulation into more environmentally stable materials. BN is ideally suited for this task as it is highly stability, while also possessing an atomically flat surface, thereby avoiding large-scale buckling of the adsorbed material which might otherwise negatively influence its properties. While the in-

fluence of BN-adsorption on the properties of graphene has been widely studied in the literature [127, 337–342], the interaction between phosphorene and BN had only been investigated systematically at the DFT level [343–347] with non of the studies addressing the effects of screening on the phosphorene band gap. The last fact that made the phosphorene/BN system a particularly interesting target was that, at the DFT level, BN adsorption was shown to result in an increase in the phosphorene band gap. Given the long-range nature of screening effects which tend to suppress the band gap of adsorbed species, I speculated that competing long and short range effects, acting on phosphorene within the phosphorene/BN system, might potentially be exploited in order to create devices whose band gap could be controlled by varying the phosphorene-BN interlayer distance. This effect could then in turn be used to create nanoscale, pressure sensitive devices. To study this, I performed a scan of the phosphorene band gap as a function of the interlayer distance in the aforementioned bilayers at different levels of theory. As expected, G_0W_0 band gaps were found to be larger than those obtained from DFT. More interestingly though, while DFT gaps showed the expected smooth convergence towards the value obtained for the isolated phosphorene monolayer, G_0W_0 band gaps were found to dip below the isolated phosphorene band gap at interlayer distance of ≈ 4 Å, indicating the presence of competing long- and short-range effects. I then investigated the effect of introducing additional BN layers to the system, either on the same site as the first BN (phosphorene/BN/BN), or on the site opposite to it (BN/phosphorene/BN). While the addition of a second BN layer below the first was found to only slightly decrease the phosphorene band gap with respect to the phosphorene/BN bilayer, its encapsulation between two BN layers resulted in a further increase of the band gap by an amount close to that observed for the addition of the first layer to pristine phosphorene. In my study I also proposed the use of the GLLB-SC potential as a starting point for G_0W_0 calculations, yielding, in the case of phosphorene, results close to those obtained from computationally more demanding GW_0@PBE calcula-

tions at the same cost as G_0W_0@PBE. The results of this study were published in paper M6.

Herein I have demonstrated how selective functionalization of graphene can be used to create materials with potential applications ranging from photovoltaics to chemical sensing. Given the shear endless number of possible graphene derivatives it stands to reason that their continued exploration will reveal many more fascinating materials and theoretical studies such as this one can and will play an important role in this endeavor, both by complementing experimental research on known materials as well as by proposing and investigating previously unknown structures.

Bibliography

[1] K. S. Novoselov, *Science* **2004**, *306*, 666–669.

[2] P. R. Wallace, *Phys. Rev.* **1947**, *71*, 622–634.

[3] R. Peierls, *Ann. Inst. Poincaré* **1935**, *5*, 177–222.

[4] L. D. Landau, *Phys. Z. Sowjetunion* **1937**, *11*, 26–35.

[5] L. D. Landau, E. M. Lifshitz, L. P. Pitaevskiĭ, *Statistical physics. Part 1, Vol. 5*, Pergamon, **1980**.

[6] A. K. Geim, K. S. Novoselov, *Nat. Mater.* **2007**, *6*, 183–191.

[7] B. Duplantier in *Statistical Mechanics of Membranes and Surfaces*, World Scientific Pub Co Pte Ltd., **2004**, pp. 245–273.

[8] J. C. Meyer, A. K. Geim, M. I. Katsnelson, K. S. Novoselov, T. J. Booth, S. Roth, *Nature* **2007**, *446*, 60–63.

[9] N. D. Mermin, *Phys. Rev.* **1968**, *176*, 250–254.

[10] A. Lipp, K. Schwetz, K. Hunold, *J. Eur. Ceram. Soc.* **1989**, *5*, 3–9.

[11] Y. Kimura, T. Wakabayashi, K. Okada, T. Wada, H. Nishikawa, *Wear* **1999**, *232*, 199–206.

[12] D.-H. Cho, J.-S. Kim, S.-H. Kwon, C. Lee, Y.-Z. Lee, *Wear* **2013**, *302*, 981–986.

[13] F. J. Clauss, *Solid lubricants and self-lubricating solids*, Elsevier, **2012**.

[14] P. Atkins, *Shriver and Atkins' inorganic chemistry*, Oxford University Press, USA, **2010**.

[15] G. L. Miessler, D. A. Tarr, *Inorganic Chemistry (3rd Edition)*, Prentice Hall, **2003**.

[16] B. Radisavljevic, A. Radenovic, J. Brivio, V. Giacometti, A. Kis, *Nat. Nanotechnol.* **2011**, *6*, 147–150.

[17] Y. Li, H. Wang, L. Xie, Y. Liang, G. Hong, H. Dai, *J. Am. Chem. Soc.* **2011**, *133*, 7296–7299.

[18] A. Splendiani, L. Sun, Y. Zhang, T. Li, J. Kim, C.-Y. Chim, G. Galli, F. Wang, *Nano Lett.* **2010**, *10*, 1271–1275.

[19] K. F. Mak, K. He, J. Shan, T. F. Heinz, *Nat. Nanotechnol.* **2012**, *7*, 494–498.

[20] H. Zeng, J. Dai, W. Yao, D. Xiao, X. Cui, *Nat. Nanotechnol.* **2012**, *7*, 490–493.

[21] Z. Yin, H. Li, H. Li, L. Jiang, Y. Shi, Y. Sun, G. Lu, Q. Zhang, X. Chen, H. Zhang, *ACS Nano* **2012**, *6*, 74–80.

[22] H. S. S. R. Matte, A. Gomathi, A. K. Manna, D. J. Late, R. Datta, S. K. Pati, C. N. R. Rao, *Angew. Chem. Int. Ed.* **2010**, *122*, 4153–4156.

[23] Q. Xiang, J. Yu, M. Jaroniec, *J. Am. Chem. Soc.* **2012**, *134*, 6575–6578.

[24] K.-K. Liu et al., *Nano Lett.* **2012**, *12*, 1538–1544.

[25] H. Wang, L. Yu, Y.-H. Lee, Y. Shi, A. Hsu, M. L. Chin, L.-J. Li, M. Dubey, J. Kong, T. Palacios, *Nano Lett.* **2012**, *12*, 4674–4680.

[26] S. Das, H.-Y. Chen, A. V. Penumatcha, J. Appenzeller, *Nano Lett.* **2013**, *13*, 100–105.

[27] Y. Yoon, K. Ganapathi, S. Salahuddin, *Nano Lett.* **2011**, *11*, 3768–3773.

[28] F. A. Rasmussen, K. S. Thygesen, *J. Phys. Chem. C* **2015**, *119*, 13169–13183.

[29] M.-L. Tsai, S.-H. Su, J.-K. Chang, D.-S. Tsai, C.-H. Chen, C.-I. Wu, L.-J. Li, L.-J. Chen, J.-H. He, *ACS Nano* **2014**, *8*, 8317–8322.

[30] H. Liu, A. T. Neal, Z. Zhu, Z. Luo, X. Xu, D. Tománek, P. D. Ye, *ACS Nano* **2014**, *8*, 4033–4041.

[31] S. Das, W. Zhang, M. Demarteau, A. Hoffmann, M. Dubey, A. Roelofs, *Nano Lett.* **2014**, *14*, 5733–5739.

[32] Q. Peng, J. Crean, L. Han, S. Liu, X. Wen, S. De, A. Dearden, *Nanotechnol. Sci. Appl.* **2014**, 1.

[33] A. Jain, A. J. H. McGaughey, *Sci. Rep.* **2015**, *5*, 8501.

[34] X. Han, H. M. Stewart, S. A. Shevlin, C. R. A. Catlow, Z. X. Guo, *Nano Lett.* **2014**, *14*, 4607–4614.

[35] L. Liang, J. Wang, W. Lin, B. G. Sumpter, V. Meunier, M. Pan, *Nano Lett.* **2014**, *14*, 6400–6406.

[36] L. Li, Y. Yu, G. J. Ye, Q. Ge, X. Ou, H. Wu, D. Feng, X. H. Chen, Y. Zhang, *Nat. Nanotechnol.* **2014**, *9*, 372–377.

[37] J.-S. Kim, Y. Liu, W. Zhu, S. Kim, D. Wu, L. Tao, A. Dodabalapur, K. Lai, D. Akinwande, *Sci. Rep.* **2015**, *5*, 8989.

[38] A. Kara, H. Enriquez, A. P. Seitsonen, L. C. Lew Yan Voon, S. Vizzini, B. Aufray, H. Oughaddou, *Surf. Sci. Rep.* **2012**, *67*, 1–18.

[39] L. Tao, E. Cinquanta, D. Chiappe, C. Grazianetti, M. Fanciulli, M. Dubey, A. Molle, D. Akinwande, *Nat. Nanotechnol.* **2015**, *10*, 227–231.

[40] Z. Ni, Q. Liu, K. Tang, J. Zheng, J. Zhou, R. Qin, Z. Gao, D. Yu, J. Lu, *Nano Lett.* **2012**, *12*, 113–118.

[41] N. D. Drummond, V. Zólyomi, V. I. Fal'ko, *Phys. Rev. B* **2012**, *85*, 075423.

[42] B. Lalmi, H. Oughaddou, H. Enriquez, A. Kara, S. Vizzini, B. Ealet, B. Aufray, *Appl. Phys. Lett.* **2010**, *97*, 223109.

[43] A. Fleurence, R. Friedlein, T. Ozaki, H. Kawai, Y. Wang, Y. Yamada-Takamura, *Phys. Rev. Lett.* **2012**, *108*, 245501.

[44] C.-C. Liu, W. Feng, Y. Yao, *Phys. Rev. Lett.* **2011**, *107*, 076802.

[45] P. Vogt, P. De Padova, C. Quaresima, J. Avila, E. Frantzeskakis, M. C. Asensio, A. Resta, B. Ealet, G. Le Lay, *Phys. Rev. Lett.* **2012**, *108*, 155501.

[46] F.-f. Zhu, W.-j. Chen, Y. Xu, C.-l. Gao, D.-d. Guan, C.-h. Liu, D. Qian, S.-C. Zhang, J.-f. Jia, *Nat. Mater.* **2015**, *14*, 1020–1025.

[47] S. Balendhran, S. Walia, H. Nili, S. Sriram, M. Bhaskaran, *Small* **2014**, *11*, 640–652.

[48] P. Tang, P. Chen, W. Cao, H. Huang, S. Cahangirov, L. Xian, Y. Xu, S.-C. Zhang, W. Duan, A. Rubio, *Phys. Rev. B* **2014**, *90*, 121408.

[49] S. Rachel, M. Ezawa, *Phys. Rev. B* **2014**, *89*, 195303.

[50] Y. Ding, Y. Wang, *J. Phys. Chem. C* **2015**, *119*, 27848–27854.

[51] W. Xiong, C. Xia, Y. Peng, J. Du, T. Wang, J. Zhang, Y. Jia, *Phys. Chem. Chem. Phys.* **2016**, *18*, 6534–6540.

[52] Y. Shaidu, O. Akin-Ojo, *Comput. Mater. Sci.* **2016**, *118*, 11–15.

[53] B. Peng, H. Zhang, H. Shao, Y. Xu, X. Zhang, H. Zhu, *Sci. Rep.* **2016**, *6*, 20225.

[54] Y. Xu, P. Tang, S.-C. Zhang, *Phys. Rev. B* **2015**, *92*, 081112.

[55] X. Chen, R. Meng, J. Jiang, Q. Liang, Q. Yang, C. Tan, X. Sun, S. Zhang, T. Ren, *Phys. Chem. Chem. Phys.* **2016**, *18*, 16302–16309.

[56] M. Ezawa, *J. Phys. Soc. Jpn.* **2015**, *84*, 121003.

[57] Y. Xu, B. Yan, H.-J. Zhang, J. Wang, G. Xu, P. Tang, W. Duan, S.-C. Zhang, *Phys. Rev. Lett.* **2013**, *111*, 136804.

[58] M. Modarresi, A. Kakoee, Y. Mogulkoc, M. Roknabadi, *Comput. Mater. Sci.* **2015**, *101*, 164–167.

[59] A. Gupta, T. Sakthivel, S. Seal, *Prog. Mater. Sci.* **2015**, *73*, 44–126.

[60] C. K. Chua, M. Pumera, *Chem. Soc. Rev.* **2013**, *42*, 3222.

[61] S. Eigler, A. Hirsch, *Angew. Chem. Int. Ed.* **2014**, *53*, 7720–7738.

[62] A. Criado, M. Melchionna, S. Marchesan, M. Prato, *Angew. Chem. Int. Ed.* **2015**, *54*, 10734–10750.

[63] T. Kuila, S. Bose, A. K. Mishra, P. Khanra, N. H. Kim, J. H. Lee, *Prog. Mater. Sci.* **2012**, *57*, 1061–1105.

[64] V. Georgakilas, M. Otyepka, A. B. Bourlinos, V. Chandra, N. Kim, K. C. Kemp, P. Hobza, R. Zboril, K. S. Kim, *Chem. Rev.* **2012**, *112*, 6156–6214.

[65] A. L. Ivanovskii, *Russ. Chem. Rev.* **2012**, *81*, 571–605.

[66] J. E. Johns, M. C. Hersam, *Acc. Chem. Res.* **2013**, *46*, 77–86.

[67] F. Karlický, K. K. R. Datta, M. Otyepka, R. Zbořil, *ACS Nano* **2013**, *7*, 6434–6464.

[68] J. Tuček et al., *Nat. Commun.* **2017**, *8*, 14525.

[69] A. Bakandritsos et al., *ACS Nano* **2017**, 2982–2991.

[70] A. Setaro et al., *Nat. Commun.* **2017**, *8*, 14281.

[71] F. Karlický, R. Zbořil, M. Otyepka, *J. Chem. Phys.* **2012**, *137*, 034709.

[72] R. Zbořil, F. Karlický, A. B. Bourlinos, T. A. Steriotis, A. K. Stubos, V. Georgakilas, K. Šafářová, D. Jančík, C. Trapalis, M. Otyepka, *Small* **2010**, *6*, 2885–2891.

[73] H. L. Poh, P. Šimek, Z. Sofer, M. Pumera, *Chem. Eur. J.* **2013**, *19*, 2655–2662.

[74] M. Pykal, P. Jurečka, F. Karlický, M. Otyepka, *Phys. Chem. Chem. Phys.* **2016**, *18*, 6351–6372.

[75] R. R. Nair et al., *Small* **2010**, *6*, 2877–2884.

[76] P. Lazar, E. Otyepková, F. Karlický, K. Čépe, M. Otyepka, *Carbon* **2015**, *94*, 804–809.

[77] K. S. Novoselov, V. I. Fal'ko, L. Colombo, P. R. Gellert, M. G. Schwab, K. Kim, *Nature* **2012**, *490*, 192–200.

[78] M. Dubecký, E. Otyepková, P. Lazar, F. Karlický, M. Petr, K. Čépe, P. Banáš, R. Zbořil, M. Otyepka, *J. Phys. Chem. Lett.* **2015**, *6*, 1430–1434.

[79] D. D. Chronopoulos, A. Bakandritsos, P. Lazar, M. Pykal, K. Čépe, R. Zbořil, M. Otyepka, *Chem. Mater.* **2017**, *29*, 926–930.

[80] J. Wu, W. Pisula, K. Müllen, *Chem. Rev.* **2007**, *107*, 718–747.

[81] L. Schmidt-Mende, *Science* **2001**, *293*, 1119–1122.

[82] A. K. Geim, I. V. Grigorieva, *Nature* **2013**, *499*, 419–425.

[83] K. S. Novoselov, A. Mishchenko, A. Carvalho, A. H. C. Neto, *Science* **2016**, *353*, 9439–9439.

[84] S. Latini, K. T. Winther, T. Olsen, K. S. Thygesen, *Nano Lett.* **2017**, *17*, 938–945.

[85] F. Withers et al., *Nat. Mater.* **2015**, *14*, 301–306.

[86] P. Rivera et al., *Nat. Commun.* **2015**, *6*, 6242.

[87] M. M. Fogler, L. V. Butov, K. S. Novoselov, *Nat. Commun.* **2014**, *5*, 4555.

[88] S. Hemmatiyan, M. Polini, A. Abanov, A. H. MacDonald, J. Sinova, *Phys. Rev. B* **2014**, *90*, 035433.

[89] M. V. Kamalakar, A. Dankert, J. Bergsten, T. Ive, S. P. Dash, *Appl. Phys. Lett.* **2014**, *105*, 212405.

[90] M. V. Kamalakar, A. Dankert, P. J. Kelly, S. P. Dash, *Sci. Rep.* **2016**, *6*, 21168.

[91] F. Natali, B. Ruck, N. Plank, H. Trodahl, S. Granville, C. Meyer, W. Lambrecht, *Prog. Mater Sci.* **2013**, *58*, 1316–1360.

[92] S. Grimme, *J. Comput. Chem.* **2006**, *27*, 1787–1799.

[93] S. Grimme, J. Antony, S. Ehrlich, H. Krieg, *J. Chem. Phys.* **2010**, *132*, 154104.

[94] S. Grimme, S. Ehrlich, L. Goerigk, *J. Comput. Chem.* **2011**, *32*, 1456–1465.

[95] A. Tkatchenko, M. Scheffler, *Phys. Rev. Lett.* **2009**, *102*, 073005.

[96] Y. Zhao, N. E. Schultz, D. G. Truhlar, *J. Chem. Phys.* **2005**, *123*, 161103.

[97] Y. Zhao, D. G. Truhlar, *J. Chem. Phys.* **2006**, *125*, 194101.

[98] Y. Zhao, D. G. Truhlar, *Theor. Chem. Acc.* **2007**, *120*, 215–241.

[99] R. Peverati, D. G. Truhlar, *Phys. Chem. Chem. Phys.* **2012**, *14*, 13171.

[100] M. Dion, H. Rydberg, E. Schröder, D. C. Langreth, B. I. Lundqvist, *Phys. Rev. Lett.* **2004**, *92*, 246401.

[101] K. Lee, E. D. Murray, L. Kong, B. I. Lundqvist, D. C. Langreth, *Phys. Rev. B* **2010**, *82*, 081101.

[102] K. Berland, V. R. Cooper, K. Lee, E. Schröder, T Thonhauser, P. Hyldgaard, B. I. Lundqvist, *Rep. Prog. Phys.* **2015**, *78*, 066501.

[103] M. D. Ben, J. VandeVondele, B. Slater, *J. Phys. Chem. Lett.* **2014**, *5*, 4122–4128.

[104] T. Schäfer, B. Ramberger, G. Kresse, *J. Chem. Phys.* **2017**, *146*, 104101.

[105] A. Grüneis, PhD thesis, Universität Wien, **2011**.

[106] M. Marsman, A. Gruneis, J. Paier, G. Kresse, *J. Chem. Phys.* **2009**, *130*, 184103.

[107] A. Grüneis, M. Marsman, G. Kresse, *J. Chem. Phys.* **2010**, *133*, 074107.

[108] G. H. Booth, A. Grüneis, G. Kresse, A. Alavi, *Nature* **2012**, *493*, 365–370.

[109] J. J. Shepherd, A. Grüneis, G. H. Booth, G. Kresse, A. Alavi, *Phys. Rev. B* **2012**, *86*, 035111.

[110] J. Harl, L. Schimka, G. Kresse, *Phys. Rev. B* **2010**, *81*, 115126.

[111] J. Harl, G. Kresse, *Phys. Rev. Lett.* **2009**, *103*, 056401.

[112] J. Harl, G. Kresse, *Phys. Rev. B* **2008**, *77*, 045136.

[113] M. Kaltak, J. Klimeš, G. Kresse, *J. Chem. Theory Comput.* **2014**, *10*, 2498–2507.

[114] M. Kaltak, J. Klimeš, G. Kresse, *Phys. Rev. B* **2014**, *90*, 054115.

[115] X. Ren, P. Rinke, C. Joas, M. Scheffler, *J. Mater. Sci.* **2012**, *47*, 7447–7471.

[116] X. Ren, P. Rinke, V. Blum, J. Wieferink, A. Tkatchenko, A. Sanfilippo, K. Reuter, M. Scheffler, *New J. Phys.* **2012**, *14*, 053020.

[117] T. Olsen, K. S. Thygesen, *Phys. Rev. B* **2013**, *87*, 075111.

[118] T. Olsen, J. Yan, J. J. Mortensen, K. S. Thygesen, *Phys. Rev. Lett.* **2011**, *107*, 156401.

[119] B. Paulus, *Phys. Rep.* **2006**, *428*, 1–52.

[120] C. Müller, B. Herschend, K. Hermansson, B. Paulus, *J. Chem. Phys.* **2008**, *128*, 214701.

[121] B. Paulus, K. Rosciszewski, *Int. J. Quantum Chem.* **2009**, *109*, 3055–3062.

[122] P. Fulde, *Theor. Chem. Acc.* **2005**, *114*, 255–258.

[123] B. Paulus, *Int. J. Mod. Phys. B* **2007**, *21*, 2204–2214.

[124] C. Pisani, L. Maschio, S. Casassa, M. Halo, M. Schütz, D. Usvyat, *J. Comput. Chem.* **2008**, *29*, 2113–2124.

[125] C. Pisani, M. Schütz, S. Casassa, D. Usvyat, L. Maschio, M. Lorenz, A. Erba, *Phys. Chem. Chem. Phys.* **2012**, *14*, 7615.

[126] S. S. Erba A., Halo M., CRYSCOR09 User's manual, University of Torino, Torino, 2009 (www.cryscor.unito.it), **2014**.

[127] F. Hüser, T. Olsen, K. S. Thygesen, *Phys. Rev. B* **2013**, *87*, 235132.

[128] M. Shishkin, G. Kresse, *Phys. Rev. B* **2006**, *74*, 035101.

[129] M. Shishkin, M. Marsman, G. Kresse, *Phys. Rev. Lett.* **2007**, *99*, 246403.

[130] M. Shishkin, G. Kresse, *Phys. Rev. B* **2007**, *75*, 235102.

[131] M. Rohlfing, S. G. Louie, *Phys. Rev. B* **2000**, *62*, 4927–4944.

[132] T. Olsen, S. Latini, F. Rasmussen, K. S. Thygesen, *Phys. Rev. Lett.* **2016**, *116*, 056401.

[133] M. Rohlfing, S. G. Louie, *Phys. Rev. Lett.* **1998**, *81*, 2312–2315.

[134] S. Albrecht, L. Reining, R. D. Sole, G. Onida, *Phys. Rev. Lett.* **1998**, *80*, 4510–4513.

[135] F. Fuchs, J. Furthmüller, F. Bechstedt, M. Shishkin, G. Kresse, *Phys. Rev. B* **2007**, *76*, 115109.

[136] J. Deslippe, G. Samsonidze, D. A. Strubbe, M. Jain, M. L. Cohen, S. G. Louie, *Comput. Phys. Commun.* **2012**, *183*, 1269–1289.

[137] M. S. Hybertsen, S. G. Louie, *Phys. Rev. B* **1986**, *34*, 5390–5413.

[138] X. Gonze, *Z. Kristallogr. Cryst. Mater.* **2005**, *220*, 2194–4946.

[139] A. Gulans, S. Kontur, C. Meisenbichler, D. Nabok, P. Pavone, S. Rigamonti, S. Sagmeister, U. Werner, C. Draxl, *J. Phys. Condens. Matter* **2014**, *26*, 363202.

[140] M. Govoni, G. Galli, *J. Chem. Theory Comput.* **2015**, *11*, 2680–2696.

[141] H. Jiang, P. Blaha, *Phys. Rev. B* **2016**, *93*, 115203.

[142] A. Marini, C. Hogan, M. Grüning, D. Varsano, *Comput. Phys. Commun.* **2009**, *180*, 1392–1403.

[143] C. Friedrich, S. Blügel, A. Schindlmayr, *Phys. Rev. B* **2010**, *81*, 125102.

[144] L. Martin-Samos, G. Bussi, *Comput. Phys. Commun.* **2009**, *180*, 1416–1425.

[145] P. Giannozzi et al., *J. Phys. Condens. Matter* **2009**, *21*, 395502.

[146] X. Blase, C. Attaccalite, V. Olevano, *Phys. Rev. B* **2011**, *83*, 115103.

[147] F. Caruso, P. Rinke, X. Ren, A. Rubio, M. Scheffler, *Phys. Rev. B* **2013**, *88*, 075105.

[148] P. A. M. Dirac, *Proc. R. Soc. A* **1929**, *123*, 714–733.

[149] E. Schrödinger, *Ann. Phys. (Leipzig)* **1926**, *81*, 109.

[150] M. Born, R. Oppenheimer, *Ann. Phys. (Berlin)* **1927**, *389*, 457–484.

[151] J. C. Slater, *Phys. Rev.* **1951**, *81*, 385–390.

[152] A. Szabo, N. S. Ostlund, *Modern quantum chemistry: introduction to advanced electronic structure theory*, Courier Corporation, **1989**.

[153] W. Kohn, L. J. Sham, *Phys. Rev.* **1965**, *140*, A1133–A1138.

[154] P. Hohenberg, W. Kohn, *Phys. Rev.* **1964**, *136*, B864–B871.

[155] C. C. J. Roothaan, *Rev. Mod. Phys.* **1951**, *23*, 69–89.

[156] G. G. Hall, *Proc. R. Soc. A* **1951**, *205*, 541–552.

[157] R. Dovesi et al., *Int. J. Quantum Chem.* **2014**, *114*, 1287–1317.

[158] R. Dovesi et al., *University of Torino Torino* **2014**.

[159] T. Helgaker, P. Jorgensen, J. Olsen, *Molecular electronic-structure theory*, John Wiley & Sons, **2014**.

[160] M. Causa, R. Dovesi, R. Orlando, C. Pisani, V. R. Saunders, *J. Phys. Chem.* **1988**, *92*, 909–913.

[161] T. C. Koopmans, *Physica* **1934**, *1*, 104–113.

[162] R. G. Parr, R. S. Mulliken, *J. Chem. Phys.* **1950**, *18*, 1338–1346.

[163] M. Jungen, *Theoret. Chim. Acta* **1981**, *60*, 369–377.

[164] M. Levy, *Proc. Natl. Acad. Sci. U.S.A.* **1979**, *76*, 6062–6065.

[165] M. Levy in *Adv. Quantum Chem.* Elsevier, **1990**, pp. 69–95.

[166] M. Kuisma, J. Ojanen, J. Enkovaara, T. T. Rantala, *Phys. Rev. B* **2010**, *82*, 115106.

[167] J. P. Perdew, R. G. Parr, M. Levy, J. L. Balduz, *Phys. Rev. Lett.* **1982**, *49*, 1691–1694.

[168] J. P. Perdew in AIP Conference Proceedings, AIP Publishing, **2001**.

[169] D. M. Ceperley, B. J. Alder, *Phys. Rev. Lett.* **1980**, *45*, 566–569.

[170] P. A. M. Dirac in Math. Proc. Cambridge Philos. Soc, *Vol. 26*, Cambridge University Press (CUP), **1930**, p. 376.

[171] S. H. Vosko, L. Wilk, M. Nusair, *Can. J. Phys.* **1980**, *58*, 1200–1211.

[172] R. G. Parr in *Horizons of Quantum Chemistry*, Springer Nature, **1980**, pp. 5–15.

[173] J. P. Perdew, A. Zunger, *Phys. Rev. B* **1981**, *23*, 5048–5079.

[174] T. Chachiyo, *J. Chem. Phys.* **2016**, *145*, 021101.

[175] J. P. Perdew, Y. Wang, *Phys. Rev. B* **1992**, *45*, 13244–13249.

[176] J. P. Perdew, K. Burke, M. Ernzerhof, *Phys. Rev. Lett.* **1996**, *77*, 3865–3868.

[177] Y. Zhang, W. Yang, *Phys. Rev. Lett.* **1998**, *80*, 890–890.

[178] B. Hammer, L. B. Hansen, J. K. Nørskov, *Phys. Rev. B* **1999**, *59*, 7413–7421.

[179] J. P. Perdew, A. Ruzsinszky, G. I. Csonka, O. A. Vydrov, G. E. Scuseria, L. A. Constantin, X. Zhou, K. Burke, *Phys. Rev. Lett.* **2008**, *100*, 136406.

[180] A. D. Becke, *J. Chem. Phys.* **1993**, *98*, 1372–1377.

[181] C. Adamo, V. Barone, *J. Chem. Phys.* **1999**, *110*, 6158–6170.

[182] A. D. Becke, *Phys. Rev. A* **1988**, *38*, 3098–3100.

[183] C. Lee, W. Yang, R. G. Parr, *Phys. Rev. B* **1988**, *37*, 785–789.

[184] K. Kim, K. D. Jordan, *J. Chem. Phys.* **1994**, *98*, 10089–10094.

[185] P. J. Stephens, F. J. Devlin, C. F. Chabalowski, M. J. Frisch, *J. Phys. Chem.* **1994**, *98*, 11623–11627.

[186] J. Heyd, G. E. Scuseria, M. Ernzerhof, *J. Chem. Phys.* **2003**, *118*, 8207–8215.

[187] J. Heyd, G. E. Scuseria, *J. Chem. Phys.* **2004**, *121*, 1187–1192.

[188] J. E. Moussa, P. A. Schultz, J. R. Chelikowsky, *J. Chem. Phys.* **2012**, *136*, 204117.

[189] K. Berland, P. Hyldgaard, *Phys. Rev. B* **2014**, *89*, 035412.

[190] O. Gritsenko, R. van Leeuwen, E. van Lenthe, E. J. Baerends, *Phys. Rev. A* **1995**, *51*, 1944–1954.

[191] R. T. Sharp, G. K. Horton, *Phys. Rev.* **1953**, *90*, 317–317.

[192] J. D. Talman, W. F. Shadwick, *Phys. Rev. A* **1976**, *14*, 36–40.

[193] M. Städele, J. A. Majewski, P. Vogl, A. Görling, *Phys. Rev. Lett.* **1997**, *79*, 2089–2092.

[194] J. B. Krieger, Y. Li, G. J. Iafrate, *Phys. Rev. A* **1992**, *45*, 101–126.

[195] I. E. Castelli, T. Olsen, S. Datta, D. D. Landis, S. Dahl, K. S. Thygesen, K. W. Jacobsen, *Energy Environ. Sci.* **2012**, *5*, 5814–5819.

[196] A. Seidl, A. Görling, P. Vogl, J. A. Majewski, M. Levy, *Phys. Rev. B* **1996**, *53*, 3764–3774.

[197] H. R. Eisenberg, R. Baer, *Phys. Chem. Chem. Phys.* **2009**, *11*, 4674.

[198] R. J. Bartlett, J. F. Stanton in *Rev. Comput. Chem.* Wiley-Blackwell, pp. 65–169.

[199] X.-Z. Li, R. Gómez-Abal, H. Jiang, C. Ambrosch-Draxl, M. Scheffler, *New J. Phys.* **2012**, *14*, 023006.

[200] F. Aryasetiawan, O. Gunnarsson, *Rep. Prog. Phys.* **1998**, *61*, 237–312.

[201] R. D. Mattuck, *A Guide to Feynman Diagrams in the Many-Body Problem: Second Edition*, Dover Publications, **1992**.

[202] C. Møller, M. S. Plesset, *Phys. Rev.* **1934**, *46*, 618–622.

[203] J. Olsen, O. Christiansen, H. Koch, P. Jørgensen, *J. Chem. Phys.* **1996**, *105*, 5082–5090.

[204] R. F. Fink, *J. Chem. Phys.* **2016**, *145*, 184101.

[205] D. L. Freeman, *J. Phys. Condens. Matter* **1983**, *16*, 711–727.

[206] D. Bohm, D. Pines, *Phys. Rev.* **1951**, *82*, 625–634.

[207] D. Pines, D. Bohm, *Phys. Rev.* **1952**, *85*, 338–353.

[208] D. Bohm, D. Pines, *Phys. Rev.* **1953**, *92*, 609–625.

[209] G. E. Scuseria, T. M. Henderson, D. C. Sorensen, *J. Chem. Phys.* **2008**, *129*, 231101.

[210] D. L. Freeman, *Phys. Rev. B* **1977**, *15*, 5512–5521.

[211] J. Paier, B. G. Janesko, T. M. Henderson, G. E. Scuseria, A. Grüneis, G. Kresse, *J. Chem. Phys.* **2010**, *132*, 094103.

[212] A. Grüneis, M. Marsman, J. Harl, L. Schimka, G. Kresse, *J. Chem. Phys.* **2009**, *131*, 154115.

[213] T. Helgaker, P. Jørgensen, J. Olsen, *Molecular Electronic-Structure Theory*, Wiley-Blackwell, **2000**.

[214] P. Pulay, *Chem. Phys. Lett.* **1983**, *100*, 151–154.

[215] P. Pulay, S. Saebø, *Theor. Chem. Acta* **1986**, *69*, 357–368.

[216] S. Saebø, P. Pulay, *J. Chem. Phys.* **1987**, *86*, 914–922.

[217] J. M. Foster, S. F. Boys, *Rev. Mod. Phys.* **1960**, *32*, 300–302.

[218] S. F. Boys, *Rev. Mod. Phys.* **1960**, *32*, 296–299.

[219] J. Pipek, P. G. Mezey, *J. Chem. Phys.* **1989**, *90*, 4916–4926.

[220] D. Usvyat, L. Maschio, M. Schütz, *J. Chem. Phys.* **2015**, *143*, 102805.

[221] M. Schütz, J. Yang, G. K.-L. Chan, F. R. Manby, H.-J. Werner, *J. Chem. Phys.* **2013**, *138*, 054109.

[222] J. Yang, G. K.-L. Chan, F. R. Manby, M. Schütz, H.-J. Werner, *J. Chem. Phys.* **2012**, *136*, 144105.

[223] Y. Kurashige, J. Yang, G. K.-L. Chan, F. R. Manby, *J. Chem. Phys.* **2012**, *136*, 124106.

[224] J. Yang, Y. Kurashige, F. R. Manby, G. K. L. Chan, *J. Chem. Phys.* **2011**, *134*, 044123.

[225] L. Hedin, *Phys. Rev.* **1965**, *139*, A796–A823.

[226] R. W. Godby, M. Schlüter, L. J. Sham, *Phys. Rev. Lett.* **1986**, *56*, 2415–2418.

[227] M. S. Hybertsen, S. G. Louie, *Phys. Rev. Lett.* **1985**, *55*, 1418–1421.

[228] F. Caruso, PhD dissertation, Freie Universität Berlin, **2013**.

[229] F. A. Rasmussen, PhD dissertation, Technical University of Denmark, **2016**.

[230] G. Antonius, Plot beautiful Feynman diagrams with matplotlib. http://github.com/GkAntonius/feynman, Accessed: 2017-02-27.

[231] F. Hüser, PhD dissertation, Technical University of Denmark, **2013**.

[232] M. van Schilfgaarde, T. Kotani, S. Faleev, *Phys. Rev. Lett.* **2006**, *96*, 226402.

[233] T. Kotani, M. van Schilfgaarde, S. V. Faleev, A. Chantis, *J. Phys. Condens. Matter* **2007**, *19*, 365236.

[234] H. J. de Groot, P. A. Bobbert, W. van Haeringen, *Phys. Rev. B* **1995**, *52*, 11000–11007.

[235] F. Bruneval, F. Sottile, V. Olevano, R. Del Sole, L. Reining, *Phys. Rev. Lett.* **2005**, *94*, 186402.

[236] P. Romaniello, S. Guyot, L. Reining, *J. Chem. Phys.* **2009**, *131*, 154111.

[237] G. D. Scholes, G. Rumbles, *Nat. Mater.* **2006**, *5*, 683–696.

[238] G. Onida, L. Reining, A. Rubio, *Rev. Mod. Phys.* **2002**, *74*, 601–659.

[239] H. Bethe, E. Salpeter, *Phys. Rev.* **1951**, *82*, 291–346.

[240] L. Reining, V. Olevano, A. Rubio, G. Onida, *Phys. Rev. Lett.* **2002**, *88*, 066404.

[241] B.-C. Shih, Y. Xue, P. Zhang, M. L. Cohen, S. G. Louie, *Phys. Rev. Lett.* **2010**, *105*, 146401.

[242] C. Friedrich, M. C. Müller, S. Blügel, *Phys. Rev. B* **2011**, *83*, 081101.

[243] T. Kato, *Comm. Pure Appl. Math.* **1957**, *10*, 151–177.

[244] C. Schwartz, *Phys. Rev.* **1962**, *126*, 1015–1019.

[245] W. Kutzelnigg, J. D. Morgan, *J. Chem. Phys.* **1992**, *96*, 4484–4508.

[246] R. A. Kendall, T. H. Dunning, R. J. Harrison, *J. Chem. Phys.* **1992**, *96*, 6796–6806.

[247] A. Halkier, T. Helgaker, P. Jørgensen, W. Klopper, H. Koch, J. Olsen, A. K. Wilson, *Chem. Phys. Lett.* **1998**, *286*, 243–252.

[248] A. Schindlmayr, *Phys. Rev. B* **2013**, *87*, 075104.

[249] J. Klimeš, M. Kaltak, G. Kresse, *Phys. Rev. B* **2014**, *90*, 075125.

[250] D. Nabok, A. Gulans, C. Draxl, *Phys. Rev. B* **2016**, *94*, 035118.

[251] F. H. da Jornada, D. Y. Qiu, S. G. Louie, *Phys. Rev. B* **2017**, *95*, 035109.

[252] D. Y. Qiu, F. H. da Jornada, S. G. Louie, *Phys. Rev. B* **2016**, *93*, 235435.

[253] D. Y. Qiu, F. H. da Jornada, S. G. Louie, *Phys. Rev. Lett.* **2013**, *111*, 216805.

[254] L. Yang, J. Deslippe, C.-H. Park, M. L. Cohen, S. G. Louie, *Phys. Rev. Lett.* **2009**, *103*, 186802.

[255] M. M. Ugeda et al., *Nat. Mater.* **2014**, *13*, 1091–1095.

[256] J Enkovaara et al., *J. Phys. Condens. Matter* **2010**, *22*, 253202.

[257] J. J. Mortensen, L. B. Hansen, K. W. Jacobsen, *Phys. Rev. B* **2005**, *71*, 035109.

[258] C. A. Rozzi, D. Varsano, A. Marini, E. K. U. Gross, A. Rubio, *Phys. Rev. B* **2006**, *73*, 205119.

[259] F. A. Rasmussen, P. S. Schmidt, K. T. Winther, K. S. Thygesen, *Phys. Rev. B* **2016**, *94*, 155406.

[260] S. Latini, T. Olsen, K. S. Thygesen, *Phys. Rev. B* **2015**, *92*, 245123.

[261] C. D. Sherrill, H. F. Schaefer in *Adv. Quantum Chem.* Elsevier BV, **1999**, pp. 143–269.

[262] M. Lorenz, D. Usvyat, M. Schütz, *J. Chem. Phys.* **2011**, *134*, 094101.

[263] M. Lorenz, L. Maschio, M. Schütz, D. Usvyat, *J. Chem. Phys.* **2012**, *137*, 204119.

[264] S. Latini, PhD dissertation, Technical University of Denmark, **2016**.

[265] P. E. Blöchl, *Phys. Rev. B* **1994**, *50*, 17953–17979.

[266] K. Lejaeghere et al., *Science* **2016**, *351*, aad3000–aad3000.

[267] T. H. Dunning, *J. Chem. Phys.* **1989**, *90*, 1007–1023.

[268] D. E. Woon, T. H. Dunning, *J. Chem. Phys.* **1993**, *98*, 1358–1371.

[269] F. Weigend, R. Ahlrichs, *Phys. Chem. Chem. Phys.* **2005**, *7*, 3297.

[270] F. Jensen, *J. Chem. Phys.* **2001**, *115*, 9113–9125.

[271] F. Jensen, *J. Chem. Phys.* **2002**, *116*, 7372–7379.

[272] F. Jensen, *J. Chem. Phys.* **2002**, *117*, 9234–9240.

[273] F. Jensen, *J. Chem. Phys.* **2003**, *118*, 2459.

[274] F. Jensen, T. Helgaker, *J. Chem. Phys.* **2004**, *121*, 3463–3470.

[275] M. F. Peintinger, D. V. Oliveira, T. Bredow, *J. Comput. Chem.* **2012**, *34*, 451–459.

[276] H. Preuss, *Z. Naturforsch. A* **1956**, *11*, 823–831.

[277] S. F. Boys, *Proc. R. Soc. A* **1950**, *200*, 542–554.

[278] S. F. Boys, G. B. Cook, C. M. Reeves, I. Shavitt, *Nature* **1956**, *178*, 1207–1209.

[279] P. M. Gill in *Adv. Quantum Chem.* Elsevier BV, **1994**, pp. 141–205.

[280] D. E. Woon, T. H. Dunning, *J. Chem. Phys.* **1994**, *100*, 2975–2988.

[281] D. E. Woon, T. H. Dunning, *J. Chem. Phys.* **1995**, *103*, 4572–4585.

[282] A. K. Wilson, T. van Mourik, T. H. Dunning, *Comp. Theor. Chem.* **1996**, *388*, 339–349.

[283] B. P. Prascher, D. E. Woon, K. A. Peterson, T. H. Dunning, A. K. Wilson, *Theor. Chem. Acc.* **2010**, *128*, 69–82.

[284] T. V. Mourik, T. H. Dunning, *Int. J. Quantum Chem.* **2000**, *76*, 205–221.

[285] A. K. Wilson, D. E. Woon, K. A. Peterson, T. H. Dunning, *J. Chem. Phys.* **1999**, *110*, 7667–7676.

[286] T. H. Dunning, K. A. Peterson, A. K. Wilson, *J. Chem. Phys.* **2001**, *114*, 9244–9253.

[287] J. M. Soler, E. Artacho, J. D. Gale, A. García, J. Junquera, P. Ordejón, D. Sánchez-Portal, *J. Phys. Condens. Matter* **2002**, *14*, 2745–2779.

[288] E. Artacho et al., *J. Phys. Condens. Matter* **2008**, *20*, 064208.

[289] E. Artacho, J. M. Cela, J. D. Gale, A. G. a, J. Junquera, R. M. Martin, P. Ordejón, D. Sánchez-Portal, J. M. Soler, *Universidad Autónoma de Madrid Madrid* **2016**.

[290] R. P. Feynman, *Phys. Rev.* **1939**, *56*, 340–343.

[291] H. Hellmann, *Einführung in die Quantenchemie*, F. Deuticke, **1937**.

[292] J. C. Slater, *Phys. Rev.* **1937**, *51*, 846–851.

[293] P. Pulay, *Mol. Phys.* **1969**, *17*, 197–204.

[294] A. Castro, H. Appel, M. Oliveira, C. A. Rozzi, X. Andrade, F. Lorenzen, M. A. L. Marques, E. K. U. Gross, A. Rubio, *Phys. Status Solidi* **2006**, *243*, 2465–2488.

[295] P. Schwerdtfeger, *ChemPhysChem* **2011**, *12*, 3143–3155.

[296] H. Hellmann, *J. Chem. Phys.* **1935**, *3*, 61–61.

[297] S. G. Louie, S. Froyen, M. L. Cohen, *Phys. Rev. B* **1982**, *26*, 1738–1742.

[298] H. Hellmann, W. Kassatotschkin, *J. Chem. Phys.* **1936**, *4*, 324–325.

[299] D. Vanderbilt, *Phys. Rev. B* **1990**, *41*, 7892–7895.

[300] G. B. Bachelet, D. R. Hamann, M. Schlüter, *Phys. Rev. B* **1982**, *26*, 4199–4228.

[301] D. R. Hamann, M. Schlüter, C. Chiang, *Phys. Rev. Lett.* **1979**, *43*, 1494–1497.

[302] D. Andrae, U. Häußermann, M. Dolg, H. Stoll, H. Preuß, *Theor. Chem. Acc.* **1990**, *77*, 123–141.

[303] S. Lebègue, B. Arnaud, M. Alouani, P. E. Bloechl, *Phys. Rev. B* **2003**, *67*, 155208.

[304] C. Rostgaard, *arXiv preprint arXiv:0910.1921* **2009**.

[305] M. Marsman, G. Kresse, *J. Chem. Phys.* **2006**, *125*, 104101.

[306] M. Valiev et al., *Comput. Phys. Commun.* **2010**, *181*, 1477–1489.

[307] M. Torrent, F. Jollet, F. Bottin, G. Zérah, X. Gonze, *Comput. Mater. Sci.* **2008**, *42*, 337–351.

[308] T. Rangel, D. Caliste, L. Genovese, M. Torrent, *Comput. Phys. Commun.* **2016**, *208*, 1–8.

[309] G. Kresse, J. Furthmüller, *Comput. Mater. Sci.* **1996**, *6*, 15–50.

[310] G. Kresse, J. Hafner, *Phys. Rev. B* **1994**, *49*, 14251–14269.

[311] G. Kresse, J. Hafner, *Phys. Rev. B* **1993**, *47*, 558–561.

[312] G. Kresse, D. Joubert, *Phys. Rev. B* **1999**, *59*, 1758–1775.

[313] M. Paulsson, *arXiv preprint cond-mat/0210519* **2002**.

[314] W. A. G. III, D. Brenner, S. E. Lyshevski, G. J. Iafrate, *Handbook of Nanoscience, Engineering, and Technology*, CRC Press, **2002**.

[315] M. A. Reed, T. Lee, *Molecular Nanoelectronics*, American Scientific Publishers, **2003**.

[316] H. Morkoc, *Advanced Semiconductors and Organic Nano-Techniques*, Academic press, **2002**.

[317] S. Datta, *Electronic Transport In Mesoscopic Systems*, Cambridge University Press, **1997**.

[318] S. Rühle, *Solar Energy* **2016**, *130*, 139–147.

[319] F. Karlický, M. Otyepka, *J. Chem. Theory Comput.* **2013**, *9*, 4155–4164.

[320] A. I. Podlivaev, L. A. Openov, *Semiconductors* **2011**, *45*, 958–961.

[321] H. Shayan, PhD dissertation, Texas A& M University, **2016**.

[322] E. Şaşıoğlu, H. Hadipour, C. Friedrich, S. Blügel, I. Mertig, *Phys. Rev. B* **2017**, *95*, 060408.

[323] F. Buonocore, A. M. Conte, N. Lisi, *Physica E* **2016**, *78*, 65–72.

[324] J. Zhou, Q. Wang, Q. Sun, P. Jena, *Appl. Phys. Lett.* **2011**, *98*, 063108.

[325] C. F. Woellner, P. A. da Silva Autreto, D. S. Galvao, *arXiv preprint arXiv:1606.09235* **2016**.

[326] C. F. Woellner, P. A. da Silva Autreto, D. S. Galvao, *arXiv preprint arXiv:1601.04484* **2016**.

[327] H Şahin, M. Topsakal, S. Ciraci, *Phys. Rev. B* **2011**, *83*, 115432.

[328] S. C. Ray, N. Soin, T. Makgato, C. H. Chuang, W. F. Pong, S. S. Roy, S. K. Ghosh, A. M. Strydom, J. A. McLaughlin, *Sci. Rep.* **2014**, *4*, 3862.

[329] D. Boukhvalov, *Physica E* **2010**, *43*, 199–201.

[330] J. T. Tanskanen, L. Maschio, A. J. Karttunen, M. Linnolahti, T. A. Pakkanen, *ChemPhysChem* **2012**, *13*, 2361–2367.

[331] X. Wang, A. M. Jones, K. L. Seyler, V. Tran, Y. Jia, H. Zhao, H. Wang, L. Yang, X. Xu, F. Xia, *Nat. Nanotechnol.* **2015**, *10*, 517–521.

[332] H. Liu, A. T. Neal, Z. Zhu, Z. Luo, X. Xu, D. Tománek, P. D. Ye, *ACS Nano* **2014**, *8*, 4033–4041.

[333] J. Yang, R. Xu, J. Pei, Y. W. Myint, F. Wang, Z. Wang, S. Zhang, Z. Yu, Y. Lu, *Light Sci. Appl.* **2015**, *4*, e312.

[334] L. Li et al., *Nat. Nanotechnol.* **2016**, *12*, 21–25.

[335] S. Bagheri, N. Mansouri, E. Aghaie, *Int. J. Hydrogen Energy* **2016**, *41*, 4085–4095.

[336] J. O. Island, G. A. Steele, H. S. J. van der Zant, A. Castellanos-Gomez, *2D Mater.* **2015**, *2*, 011002.

[337] N. Kharche, S. K. Nayak, *Nano Lett.* **2011**, *11*, 5274–5278.

[338] M. Bokdam, T. Amlaki, G. Brocks, P. J. Kelly, *Phys. Rev. B* **2014**, *89*, 201404.

[339] G. Giovannetti, P. A. Khomyakov, G. Brocks, P. J. Kelly, J. van den Brink, *Phys. Rev. B* **2007**, *76*, 073103.

[340] B. Sachs, T. O. Wehling, M. I. Katsnelson, A. I. Lichtenstein, *Phys. Rev. B* **2011**, *84*, 195414.

[341] R. Quhe et al., *NPG Asia Mater.* **2012**, *4*, e6.

[342] J. Sławińska, I. Zasada, Z. Klusek, *Phys. Rev. B* **2010**, *81*, 155433.

[343] Y. Cai, G. Zhang, Y.-W. Zhang, *J. Phys. Chem. C* **2015**, *119*, 13929–13936.

[344] T. Hu, J. Hong, *ACS Appl. Mater. Interfaces* **2015**, *7*, 23489–23495.

[345] B. You, X. Wang, W. Mi, *Phys. Chem. Chem. Phys.* **2015**, *17*, 31253–31259.

[346] G. C. Constantinescu, N. D. M. Hine, *Nano Lett.* **2016**, *16*, 2586–2594.

[347] P. Zhang, J. Wang, X.-M. Duan, *Chin. Phys. B* **2016**, *25*, 037302.